LINKING RESIN CANAL AND WOOD ANATOMY IN LOBLOLLY PINE EXPERIENCING DIEBACK

by

NAWA RAJ POKHREL

(Under the Direction of Joseph Dahlen)

ABSTRACT

Resin canals are of particular importance to conifer tree defense. The study examined resin canals and wood properties of mature loblolly pine stands that were showing signs of dieback. From Georgia, seven symptomatic stands experiencing dieback and seven asymptomatic stands were sampled with the symptomatic stands sampled just prior to being clearcut. Bark-to-bark core samples were collected at breast height (1.37 m) from 10 'healthy' trees from each stand, and 10 'unhealthy' trees from each symptomatic stand. Ring by ring properties including specific gravity (SG), acoustic velocity, and resin canals were determined from the 210 cores from pith to bark. 24,865 resin canals were measured using image analysis from 24,153 images. Compared to symptomatic unhealthy trees, asymptomatic healthy trees had significantly lower earlywood SG, significantly higher latewood SG, and significantly larger resin canals. The results indicate that the trees experiencing dieback were suffering from stress which impacted their wood anatomy.

INDEX WORDS: *pine dieback, southern pine, specific gravity, tree defense, wood and fiber properties*

LINKING RESIN CANAL AND WOOD ANATOMY IN LOBLOLLY PINE EXPERIENCING DIEBACK

by

NAWA RAJ POKHREL

B.Sc., Agriculture and Forestry University, Nepal, 2017

A Thesis Submitted to the Graduate Faculty of The University of Georgia in Partial Fulfillment of the Requirements for the Degree

MASTER OF SCIENCE

ATHENS, GEORGIA

2021

LINKING RESIN CANAL AND WOOD ANATOMY IN LOBLOLLY PINE EXPERIENCING DIEBACK

by

NAWA RAJ POKHREL

Major Professor: Joseph Dahlen

Committee: Kamal Gandhi
Michael Kane

Electronic Version Approved:

Ron Walcott
Vice Provost for Graduate Education and Dean of the Graduate School
The University of Georgia
August 2021

DEDICATION

I devote this thesis to my family who have meant and continue to mean so much to me. A special sense of gratefulness goes to my loving parents, Dhundi Raj Pokhrel and Sumitra Pokhrel whose words of inspiration and push for persistence was an unremitting source to accomplish this degree.

ACKNOWLEDGEMENTS

I would like to convey my profound gratitude towards my major advisor Dr. Joseph Dahlen. I thank him for offering the opportunity to pursue MS degree and for his incredible assistance, time, direction, inspiration, and patience throughout these years. His guidance and praise have helped me grow both personally and professionally.

I am highly indebted to my committee members Drs. Kamal Gandhi and Michael Kane for their continuous supervision and constructive comments and recommendations throughout the data collection, analysis, and thesis writing process. I am very thankful to Dr. Thomas Eberhardt for guidance, timely support, and providing materials from the very start to end of the research. Additionally, I am very thankful to Bryan Simmons and Brittany Barnes for the field and laboratory work and support throughout this research.

This study was financially supported by the USFS Forest Products Laboratory whom I thank for the support. I gratefully acknowledge the support provided by the Warnell School of Forestry and Natural Resources at the University of Georgia. I am thankful to the unconditional help and support provided by my fellow graduate students in the department.

My cordial thanks go to Sameen Raut for being a great friend to overcome my first-year struggles. In addition, I am thankful to Sadikshya Sharma, Pramod Pandey, Tej Acharya, and Volkan Bektas for their continuous help, emotional support, motivation, and love. And last, but not least, I am deeply indebted to my family whose continuous love, encouragement, endurance, and moral support was the unremitting source of inspiration for this study.

TABLE OF CONTENTS

Page

LIST OF TABLES

LIST OF FIGURES

LINKING RESIN CANAL AND WOOD ANATOMY IN LOBLOLLY PINE EXPERIENCING DIEBACK

1. Introduction

Forests of the southeastern United States (U.S.) supply approximately 60% of the timber harvested in the U.S. and approximately 18% of the timber globally (Munsell and Fox 2010, Wear and Greis 2012). The major southern pines, which include loblolly pine (*Pinus taeda*), slash pine (*Pinus elliottii*), longleaf pine (*Pinus palustris*), and shortleaf pine (*Pinus echinate*), are the most important conifer species harvested in the southeastern U.S. with loblolly pine being the most important (McNulty et al. 1996, Fox et al. 2007). Loblolly pine covers 21 million hectares (Oswalt et al. 2019) from extensive planting efforts because of its high productivity, strong response to forest management treatments, and adaptability to a wide range of sites (McKeand et al. 2006, Zhao et al. 2016, Zhao et al. 2019)

In the past several decades, loblolly pine stands have experienced periodic unexpected mortality and dieback (Eckhardt et al. 2007, Eckhardt et al. 2010). Dieback is the gradual dying of trees branches, shoots, or roots-and pine dieback symptoms include yellow chlorotic needles, reduced growth, premature mortality, and root and branch death (Eckhardt et al. 2007, Eckhardt et al. 2010). Different terms have been used by researchers to refer to pine dieback and mortality phenomenon as follows: loblolly pine die-off (Brown and McDowell 1968), pine decline (Otrosina et al. 1999, Eckhardt et al. 2007), loblolly pine decline (Hess et al. 2002), pine die-back (Eckhardt and Menard 2009), and southern pine decline (Coyle et al. 2015, Eckhardt et al.

2016). The pine dieback has typically been localized in Alabama and Georgia along the fall line (transitional zone) dividing the Piedmont and Coastal Plain physiographic regions (Eckhardt et al. 2010). Pine dieback studies have focused on identifying the contributing factors to tree mortality because it is not clear what exactly is causing the dieback (Coyle et al. 2015). It has been hypothesized that pine dieback may be caused by the interaction between various abiotic (e.g., drought, windstorms, poor site/soil conditions) and biotic (e.g., insects and disease outbreaks) factors (Hanson et al. 2010, Coyle et al. 2015, Coyle et al. 2020). The fungal root pathogens, *Heterobasidion annosum, Pythium* spp., and *Leptographium* spp., and their root-feeding bark beetle vector, are all suspected causes for the dieback symptoms (Otrosina et al. 1999, Eckhardt et al. 2007).

Plants allocate and make trade-offs of their photosynthates to growth, reproduction, and defense (Coley et al. 1985, Endara et al. 2011). For example, during drought, some conifer species produce tracheids with smaller lumen diameters but thicker cell walls having lower inter-tracheid pit area to resist hydraulic failure (Hacke et al. 2001, Pittermann et al. 2006a). The trade-off of increased resistance to hydraulic failure is that the narrower diameter tracheids reduce the overall hydraulic efficiency (Hacke et al. 2001, Pittermann et al. 2006b) and the thicker cell wall tracheids require more resources to produce than thinner walled tracheids (Lauder et al. 2019). Other examples of trade-offs include trees retaining hydraulic efficiency by reducing their overall growth under severe conditions (Moran et al. 2017). Under extreme conditions, trees might choose to allocate their carbon resources into defense systems, or they might choose to invest available resources into growth and reproduction (Lauder et al. 2019). Due to trade-offs between defense, growth, and reproduction, a cost-effective way to partition

resources into defense is needed otherwise plant growth and reproduction will suffer (Levins 1968, Christiansen and Ericsson 1986, Miller and Berryman 1986).

Conifers have developed constitutive and induced defense mechanisms against biological attacks (e.g. bark beetles and associated fungi) (Zulak and Bohlmann 2010, Hood and Sala 2015), environmental disturbances (drought, fire, frost) (Krokene 2015), mechanical wounding (Lombardero et al. 2000), and climatic conditions that include variation in temperature and precipitation (Ayres 1993, Wimmer and Grabner 1997, Celedon and Bohlmann 2019). The production of resin canals is the primary defense mechanism in both constitutive and induced defense in the *Pinaceae* family (Raffa 2014). Resin canals are open, elongated tube-like intercellular spaces lined with a layer of epithelial cells, which are specialized parenchyma cells that secrete resin into the resin canal lumen (Wu and Hu 1997, Evert 2006). Epithelial cells are further surrounded by specialized parenchyma cells called subsidiaries and this combination of the resin canal, epithelial cells, and subsidiary cells forms the resin canal complex (Wiedenhoeft and Miller 2002, Cabrita 2021). The resin produced from resin canals is a complex mixture of terpenoids, resin acids, fats, waxes, and phenolic compounds which provides physical and chemical defense against damage and disturbances (Sjöstrom 1993, Raffa 2014).

There are two types of resin canals, called axial and radial resin canals, and they are distributed along the axial (vertical) and radial (horizontal) directions, respectively (Wu and Hu 1997). The size and distribution of resin canals differ between species and within species (Bailey and Faull 1934, Wu and Hu 1997). In *Pinus* species, the dimensions of axial resin canals range from 60-300 μm in diameter (Wimmer et al. 1999) and more than 1 cm in length (LaPasha and Wheeler 1990). Axial resin canals are generally 3-4 times wider than radial resin canals (Koch 1972, Richter et al 2004). The density of axial (4-5 canals mm^{-2}) and radial resin (0.5-2 canals

mm^{-2}) canals are higher in *Pinus* species than *Larix*, *Picea*, and *Cathaya* species (Koch 1972, Cabrita 2021).

Resin canal formation and resin flow is induced by external factors such as mechanical wounding, environmental stress, biotic attack, chemical stimulants and hormones (Ruel et al. 1998, Moreira et al. 2012). The formation of resin canals that are induced by damage and wounding of the vascular cambium are called traumatic resin ducts and form from disturbances (Lombardero et al. 2000). Constitutive resin ducts are naturally formed during the development of secondary xylem and their formation is determined by genetics and prior history (Franceschi et al 2005, Krokene 2015). Traumatic resin ducts differ from constitutive resin ducts in the structure; traumatic resin ducts are tangentially and consecutively aligned and usually longer and wider than constitutive resin ducts (Nagy et al. 2000, Krokene et al 2008). The constitutive resin ducts protect trees against initial attack (Franceschi et al 2005) whereas traumatic resin ducts protect tree after an attack by supplying an abundant amount of resin in the damaged and wounded region (Keeling and Bohlmann 2006). The resin canal defense system developed from the integration between complex anatomical structures and chemical substances (Kolosova and Bohlmann 2012).

The size and frequencies of constitutive resin ducts and/or traumatic resin ducts indicate the defense potential of trees because they are associated with the production and storage capacity of resin in the tree (Kane and Kolb 2010). For example, in ponderosa pine (*Pinus ponderosa*) trees with higher resin canal production and/or larger ducts are more likely to survive under pest and pathogen attacks and drought (Kane and Kolb 2010; Gaylord et al. 2013, Gaylord et al. 2015; Hood et al. 2015). Zhao and Erbilgin (2019) found in lodgepole pine (*Pinus*

contorta) that trees that had larger resin canals were more likely to survive from bark beetle attacks, even if the trees contained fewer resin canals.

Loblolly pine trees suffering from dieback may have altered wood anatomical (e.g., tracheid length and diameter, microfibril angle), physical (e.g., specific gravity (wood density divided by the density of water), moisture content) and chemical properties (e.g., cellulose, lignin, and hemicellulose, and extractive content) (Megraw 1985; Briggs 2010) compared to 'normal' trees. Changes in the wood properties may alter the wood utilization for both structural products where high mechanical properties (e.g., stiffness and strength) are desirable (Zink-Sharp 2003) or for pulp properties where high pulp yield is desirable (Perez and Fauchon 2003). Wood SG has a strong correlation with the mechanical properties of solid wood products, and when combined with the moisture content (MC) it determines the green weight of the wood (Taras 1956, Phillips 2002). Microfibril angle (MFA) is a major determinant of longitudinal shrinkage (Meylan 1972) and longitudinal stiffness (Cave and Walker 1994). Acoustic velocity (AV) is negatively related with MFA; the measurement of AV provides a less expensive alternative compared to measuring MFA via X-ray diffraction (Hasegawa et al. 2011, Mason et al. 2017, Dahlen et al. 2019).

Assessing changes that occur in wood properties due to pine dieback requires characterization across the scales whereby variation occurs, this includes variation in site (Cregg et al. 1988), radial and vertical position, applied silviculture practices (Schimleck et al. 2018), and overall tree health (Essien et al. 2019). The largest source of variation within trees is radial variation due to cambial age changes, and then longitudinally from the stump to the top trees (Megraw et al. 1999, Zobel and van Buijtenen 2012, Melo 2015, Todoroki et al. 2015, Schimleck et al. 2020, Dahlen et al. 2021, Schimleck et al. 2021). Wood produced at young ages (near the

pith) is called corewood (juvenile wood) and wood produced at older ages is called outerwood (mature wood) (Harris and Cown 1991, Burdon et al. 2004, Zobel and Sprague 2012). Senft and Bendtsen (1986) estimated the corewood formation is the first 12 years of wood for loblolly pine. For loblolly pine, tree rings near the pith have low SG and gradually increase nonlinearly as cambial age increases (Jordan et al. 2008, Dahlen et al. 2018). For a given ring, SG will decrease with height within stem (Megraw 1985, Dahlen et al. 2018). The MFA decreases from pith to bark and for a given growth ring MFA decreases with height (Jordan et al. 2005). Because of the strong inverse relationship between MFA and AV (Hasegawa et al. 2011, Mason et al. 2017), AV will increase from pith to bark, and for a given ring will increase from stump to tip (Dahlen et al. 2019).

Information on the wood and fiber properties of symptomatic loblolly pine stands is important to better enable links between the timber and its suitability for production material. During pine dieback events, landowners will harvest stands to recover as much value as they can from the stand before significant deterioration occurs. Unfortunately, no study is available on the wood and fiber quality of trees suffering from dieback and thus information is lacking on the optimum utilization of such stands. Sampling stands suffering from dieback prevents a unique opportunity to study initial links between resin canal size and frequency and the survival of loblolly pine. This study aims to quantify and compare resin canal, and wood and fiber properties between symptomatic stands (suffering from dieback) and asymptomatic stands. We hypothesized tree suffering from pine dieback will have lower SG and MC with smaller resin ducts compared to asymptomatic stands. This study will provide a better link between forest health and wood anatomy in plantation loblolly pine.

2. Material and Methods

2.1. Sampling

Fourteen planted loblolly pine stands were sampled in 2017, with 7 asymptomatic stands and 7 symptomatic stands suffering from pine dieback selected for sampling. The stands were located near the fall line in between the Piedmont and the upper Coastal Plain regions in Georgia (Figure 1). Among seven asymptomatic stands, four were 4th row thinned, 2 were 5th row thinned and one was 3rd row thinned. From seven asymptomatic stands, six were 4th row thinned and one was first 5th row thinned. The plantation age was calculated using time series data of normalized vegetation difference index (NVDI) from the Google Earth engine (Schmid 2017).

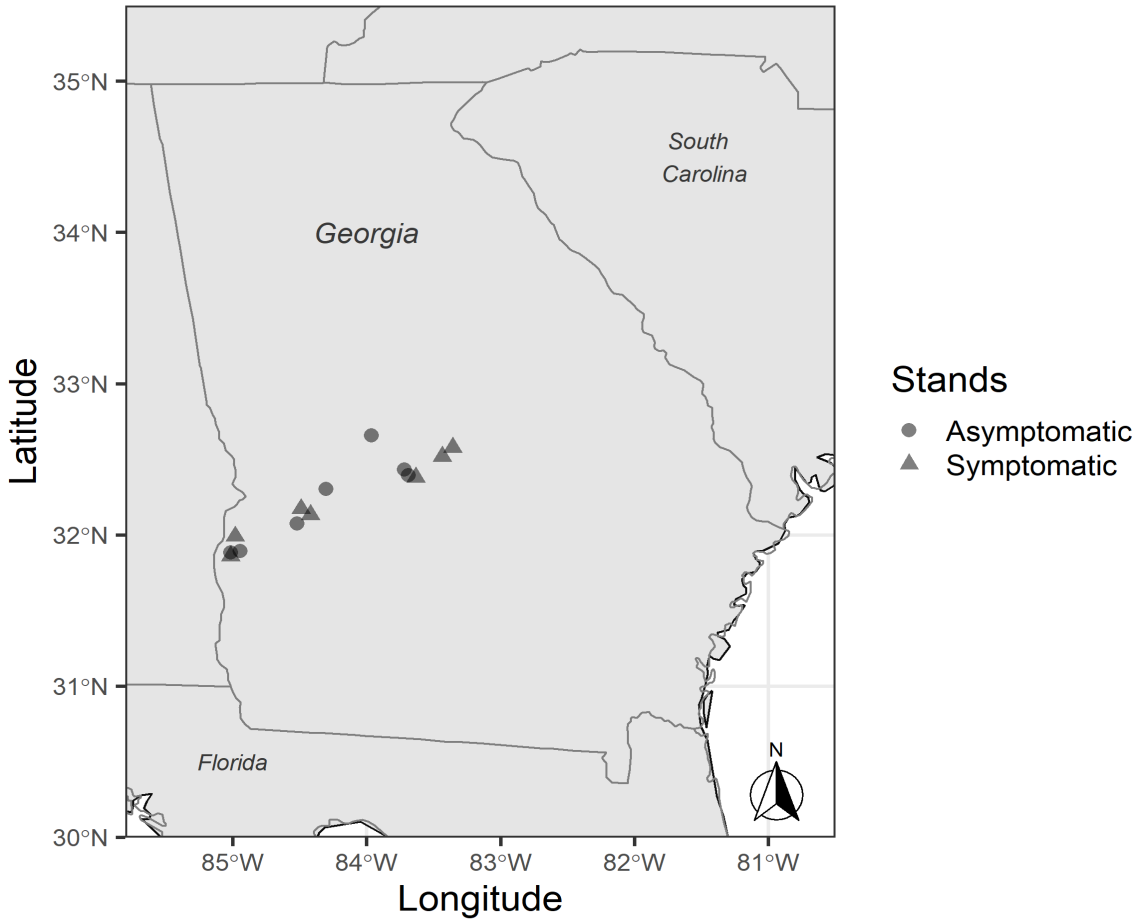

Figure 1: Sampling sites; ‘A’ represents asymptomatic stand and ‘S’ represents symptomatic stand.

An inventory was conducted within each stand to establish baseline stand characteristics, for 3 stands three 15 m fixed radius plots were established, for the remaining stands rectangular plots that included all of the sample trees were stablished. The average size rectangular plot was 1774 m^2 (SD = 1684). Within each plot, the DBH of every tree was measured, and from a subset total height and live crown ratio (ratio of crown length divided by the total height) were measured (Schomaker et al. 2007).

From each asymptomatic stand, 10 seemingly healthy trees and 10 seeming unhealthy trees were selected across the diameter distribution. The selection of the healthy trees mirrored the location (next to thin row or not) of the unhealthy trees where possible. For example, if a symptomatic tree was selected that was located next to the thinned row, then a corresponding asymptomatic tree was selected next to the thinned row. The average DBH and height of the asymptomatic trees was 29.8 cm and 20.3 m. The average DBH and height of the symptomatic healthy trees was 28.6 cm and 19.1 m. The symptomatic unhealthy trees have average DBH and height of 26.3 cm and 17.7 m. The average DBH and height were not statistically significant among the treatment groups. From the selected trees, two 12 mm bark to bark cores at breast height (1.37 m) were collected using an increment borer. The collected samples were labeled, placed individually in a plastic bag, and then frozen until processing.

Table 1: General characteristics of the sampled stands with the standard deviation values shown in parenthesis.

Stand	Latitude	Longitude	Stand conditions	Age	DBH (cm)	Height (m)	Live crown ratio (%)	Basal area (m^2 ha^{-1})	Tree per hectare	Thin row
1	32.5263	-83.3883	Symptomatic	26	27.8(4.8)	19.3(2.1)	41.4(7.6)	15.0	241	4
2	32.6144	-84.0044	Asymptomatic	24	23.1(4.5)	17.2 (2.1)	41.3(6.2)	14.9	344	5
3*	32.3735	-83.6298	Symptomatic	29	-	-	-	-	-	4
4	32.3818	-83.6499	Asymptomatic	29	31.8(3.4)	21.8 (10.3)	41.4(5.1)	18.9	235	3
5	32.3716	-83.6321	Asymptomatic	29	30.1(3.2)	22.0(11.1)	40.2(5.9)	20.8	290	4
6	31.9115	-85.0145	Symptomatic	21	24.2(4.3)	19.5(9.8)	37.8(5.3)	21.5	452	4
7	31.8895	-85.002	Asymptomatic	20	25.9(3.8)	18.7(8.9)	42.5(9.1)	18.6	348	4
8	31.9066	-85.0034	Asymptomatic	21	26.1(4.5)	21.4(10.8)	40.6(5.1)	34.5	628	4
9	32.1503	-84.4891	Symptomatic	20	25.0(6.5)	19.4(9.2)	40.1(4.1)	27.7	563	4
10	32.1349	-84.4919	Asymptomatic	20	26.0(6.8)	19.4(9.8)	39.4(4.7)	32.9	583	4
11	32.2922	-84.3356	Asymptomatic	23	26.1(3.3)	19.6(7.7)	39.1(7.4)	16.0	295	5
12	32.1581	-84.4203	Symptomatic	18	19.4(6.7)	14.5(7.4)	43.4(6.2)	13.9	481	5
13	32.5235	-83.3906	Symptomatic	26	25.3(5.4)	19.3(3.5)	46.0(6.0)	46.2	877	4
14	31.9131	-85.0109	Symptomatic	21	22.8(3.6)	18.5(9.3)	36.9(6.7)	29.1	697	4

*This stand was clearcut before an inventory could be conducted

Table 2: Characteristics of the sampled trees by treatments with the standard deviation values shown in parenthesis.

Trees	Age	DBH (cm)			Height (m)			Live Crown Ratio (%)		
	Mean	Mean	Min	Max	Mean	Min	Max	Mean	Min	Max
Asymptomatic Healthy (AH)	23.7(3.9)	29.8(5.0)	21.1	49.3	20.3(1.8)	15.7	23.9	43.7(8.1)	28.4	69.1
Symptomatic Healthy (SH)	22.5(4.1)	28.6(5.4)	20.1	46.0	19.1(2.2)	12.2	23.2	43.2(7.9)	18.8	69.0
Symptomatic unhealthy (SU)	22.5(4.1)	26.3(6.4)	15.5	49.0	17.7(2.4)	12.2	21.5	39.7(7.3)	25.5	66.2

2.2. Sample processing and data measurement

From the two bark-to-bark cores that were collected from each tree, the 'best' bark-to-bark core, having straight grain and the pith centered in the middle of the core, was selected. The selected cores were split from the pith using a razor blade mounted on a lever to yield two pith-to-bark samples. The 'best' pith-to-bark sample ('sample 1') was processed into a radial strip which was used to measure ring SG, USV, and resin canal size and frequency. The other pith-to-bark sample ('sample 2') was used to measure the whole-core specific gravity and the moisture content of the wood (Figure 2). The remaining bark-to-bark cores were stored in the freezer for possible future work.

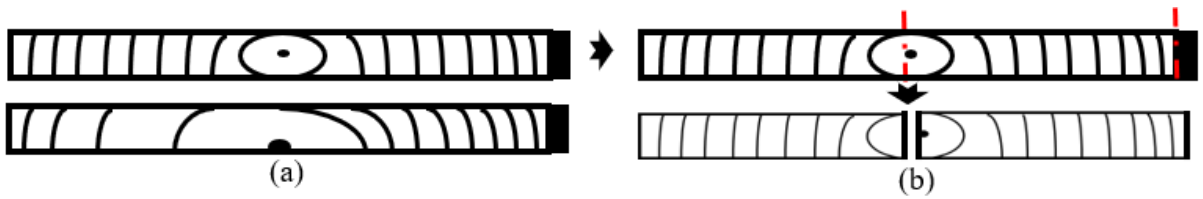

Figure 2: Sketch showing two bark-to-bark samples; a) showing two bark-to-bark samples top one with pith centered and second one showing curvature. b) splitting of best bark-to-bark sample to produce two pith-to-pith samples with 'sample 1' shown on the right.

The bark of 'sample 1' was removed and the green volume (V_g) was measured using the water displacement method following ASTM D2395 (ASTM 2017). To reduce cracking due to wood shrinkage that occurs during drying, the samples were 'dried' using 100% ethanol for three weeks whereby the ethanol displaces the water in the wood (Downes et al. 1997). The ethanol was exchanged each week with fresh ethanol. Following ethanol drying, the samples were soaked in acetone for one week to further remove resinous extractives (Eberhardt and Samuelson 2015). The samples were conditioned at 52% relative humidity and 22°C for 48 hours to achieve approximately 10% MC (Dahlen et al. 2018). The conditioned samples were weighed (W_{10}), and then the weight at 0% moisture content was estimated using ASTM D4442 (ASTM 2020):

$$W_0 = \frac{W_{10}}{1+\frac{10}{100}} \quad (1)$$

where W_0 the weight of sample at 0% moisture content, and W_{10} is weight of sample at 10% MC. The basic SG (ratio of the oven-dry weight of the sample to green volume (V_g) divided by the density of water) of the samples was calculated which was used to calibrate the X-ray densitometer.

$$SG = \frac{W_0}{V_g} \quad (2)$$

where SG is the specific gravity of the sample, W_0 is the weight of the sample at 0% moisture content, and V_g is the green volume of the samples.

The whole core SG and MC% was measured from sample '2'. The green weight (W_g) of the samples was measured and then the green volume (V_g) was measured using the water displacement method. The samples were oven-dried at 103℃ for more than 24 hours and the oven-dry weight (W_0) of the samples was measured. The basic specific gravity of the whole cores was calculated using equation 2. The MC% of the samples was calculated using:

$$MC\ (\%) = \frac{W_g - W_O}{W_O} * 100 \quad (3)$$

where MC (%) is moisture content percentage, W_g is the green weight of the samples (in grams), Wo is the oven dry weight of the samples (grams).

Ultrasonic velocity

The best samples ('1') were glued in between two poplar core holders and cut using a twin-blade table saw to yield an 8 mm thick (longitudinal) radial strip. The samples were conditioned at 52% relative humidity and 22°C for 24 hours to achieve an approximately 10%

MC. The USV of samples was measured from pith to bark on the SoniSys instrument (SoniSys, United States) at 10 mm radial resolution. Sound velocity is measured using two 1 MHz transducers by measuring the time required for a signal to be sent through the sample, combined with measurement of the thickness of the sample at the measurement point (Dahlen et al. 2019). The USV was later merged with X-ray densitometry data to assign sound velocity in each annual rings of the samples.

Figure 3: The samples layout in poplar core holders (left). The twin-blade table saw (right).

X-ray densitometry

The USV samples were then glued into a poplar holder on one transverse surface. The samples were cut from the central portion of the USV sample to yield an approximately 2 mm tangential thickness sample. The SG at 40 um radial resolution from bark to pith was measured using the QTRS-01X Tree Ring Scanner (Quintek Measurement Systems, United States) X-ray densitometer. The X-ray beam was passed through the sample on the longitudinal surface. The X-ray densitometer values were calibrated to the measured SG values. The latewood and earlywood were separated using a threshold SG value of 0.48 (Jordan et al. 2008, Antony et al. 2012, Eberhardt and Samuelson 2015). Initial ring counts of the samples were done

automatically based on the differentiation between earlywood and latewood, and then each ring was manually checked. The data from the X-ray densitometer was used to generate annual ring width, ring SG, earlywood SG, latewood SG, and latewood percent data (Antony et al. 2012, Eberhardt and Samuelson 2015).

Resin Canal Imaging

Imaging samples for resin canals requires polishing the surface. The transverse surface of the samples was sanded in a pneumatic polishing unit using 400 and 600 grit aluminum oxide sandpaper. The samples were sanded until the tracheids wall and lumen were visible. Polishing required approximately a total of 8 back and forth strokes on each grit of sandpaper before the surfaces were clear.

The samples were imaged from pith to bark in a custom-built imaging system (Figure 4). The imaging system consists of an Allied Vision G-235 monochrome camera with sensor size of 1936×1216 pixels^2 (Allied Vision, Germany) attached to an UPLFLN Olympus 4X objective microscope (Olympus, Japan). Six infrared (850 nm) LED sidelights were used to illuminate the samples. The side lights transmit the light to the polished transverse surface of the samples. The system is similar in operation to the SilviScan system (Evans 1994). Evans (1994) found that wood dust in the lumens (both tracheid and resin canals) appear dark and the tracheid cell walls are bright.

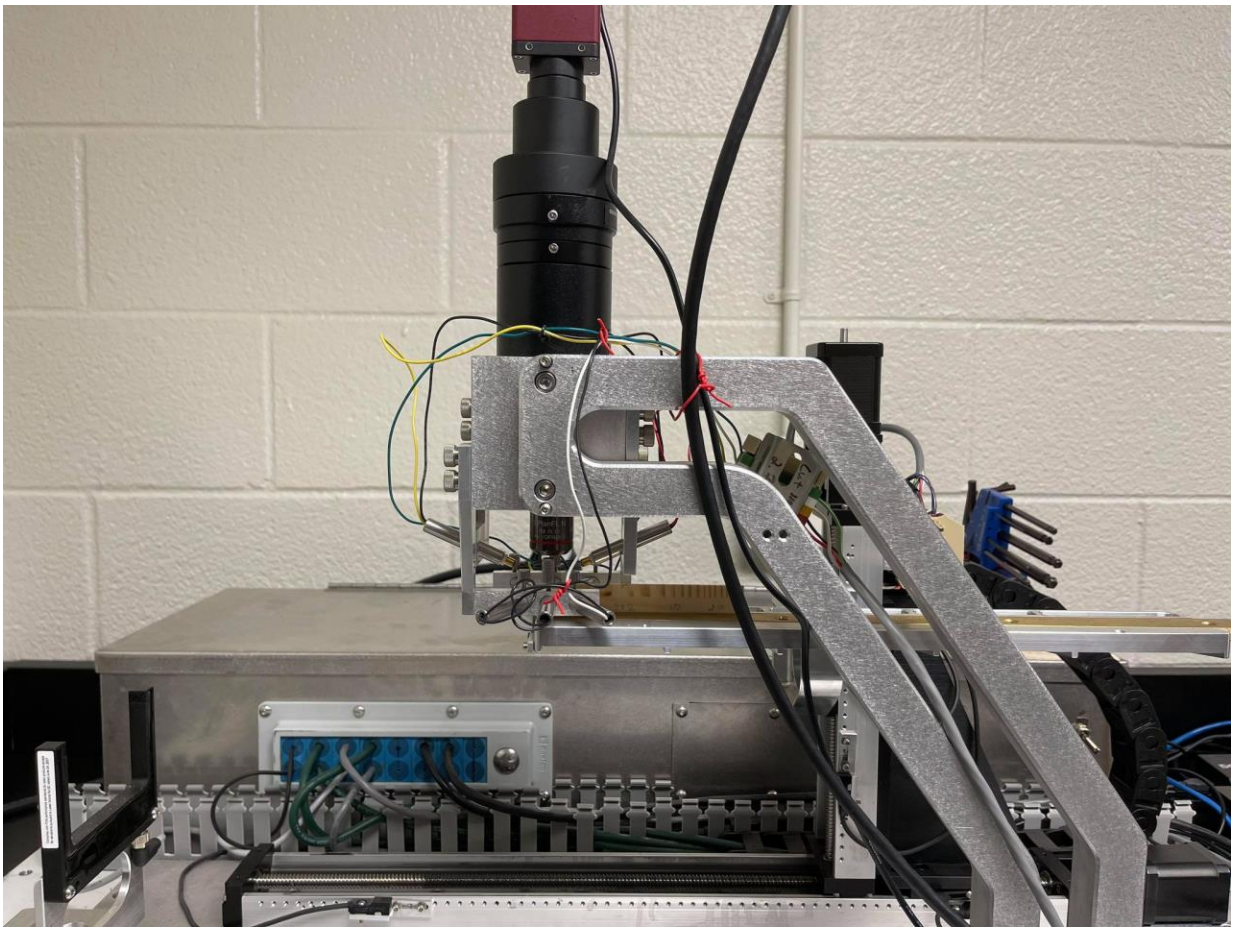

Figure 4: Imaging instrument with 4X objective lens and monochrome camera at top.

Focusing and pith to bark movement was done using two linear translation stages (X-axis and Z-axis) with stepper motors. The instrument is connected to a computer using a graphic user interface (GUI) programmed in python (Van Rossum 2007). After placing the sample in the sample holder, the height of the samples is measured using a U-shape laser sensor. The samples are then moved under the camera. The GUI automatically adjusts the contrast of the image by changing the exposure time, and the GUI also automatically adjusts the focus by changing the distance between image and the sample. The images from each sample were saved into their own unique folder, and the images were labeled in sequence from pith to bark. The images were

saved as greyscale images with 8-bit depth. The 210 samples yielded 24,153 images that contained overlapping information.

Image processing

The images were processed using Python version 3.7 (Van Tossum 2007) in the Spyder integrated development environment (IDE) (Raybaut 2009) using the libraries OpenCV (Bradski and Kaehler 2008), NumPy (Oliphant 2006), and pandas (McKinney 2010). The camera was calibrated by using a microscope stage calibration slide of 1 mm total length (AmScope, United States) (Bradski and Kaehler 2008). The calibration resulted in 1 mm of length being equal to 623 pixels.

The first and last images were cropped to remove any part of the image that did not contain sample material and instead contained 'free air'. Each image was then cropped in the radial direction to keep the central portion of the images as they are clearer than the edge of the images; the tangential image area was not cropped and thus the area imaged was equal to width of the camera sensor (1216 pixels). Except for the first and last images, the images were cropped to 668 pixels in length which represents the 668 to 1336 pixels from the original 1936 pixels of the image (Figure 5). The first images were cropped to provide any information from the start of the sample to the 668th pixel of the 2nd image. The last image was cropped from the 668th pixel to the end of the sample.

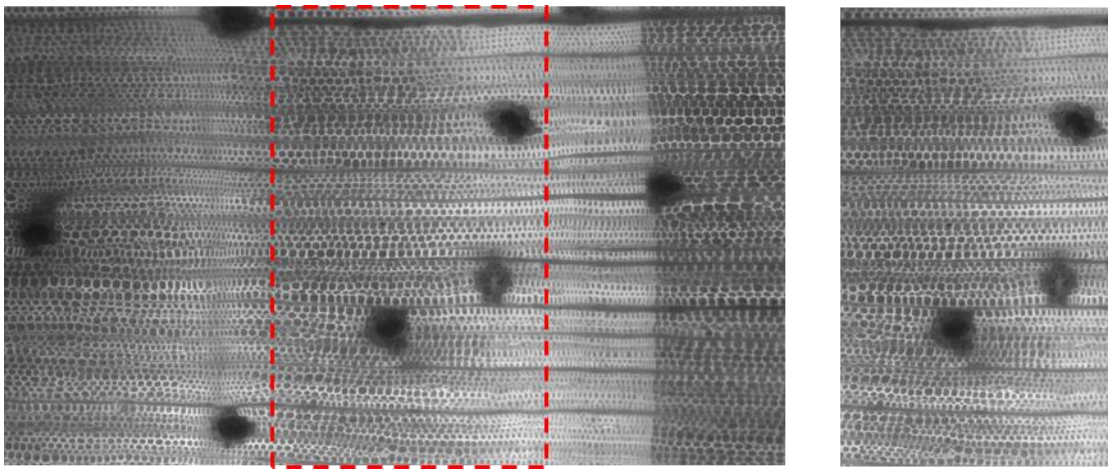

Figure 5: Image before cropping (left) and after cropping (right). Red dotted line indicates the cropped portion of image.

A series of image operations was done to improve the image quality (Figure 6). The contrast of the image was corrected by using the Contrast Limited Adaptive Histogram Equalization (CLAHE) algorithm (Pizer et al. 1990, Sasi and Jayasree 2013). Noise removal was then done by using the Non-Local Means Denoising algorithm (Motwani et al. 2004, Buades et al. 2005). The images were then converted into binary images by applying the Gaussian adaptive threshold algorithm (Rais et al. 2004). The binary images with the cell walls as bright (255-pixel value) and cell lumen as dark (0-pixel value) was then inverted.

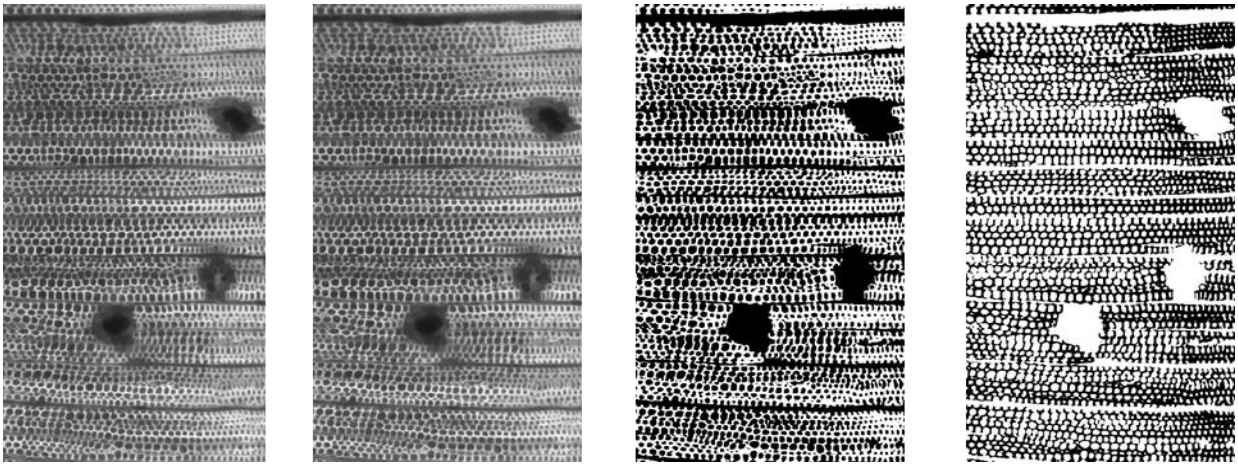

Figure 6: Image sequence from left to right: contrast corrected image, noise removed image, image after applying binary threshold, and inverted image

Morphological operations were then done on the inverted images (Figure 7), the brighter lumens (pixels value 255) were eroded to separate resin canals from any tracheid lumen. The contours were then found by using hierarchical contour retrieval models (Serra 1982). The smaller contours of the tracheid lumens, having an area of 800 pixels or less, were removed by changing the pixel values from 255 to 0. The remaining contours were then dilated to restore their original size prior to the erosion process. The above operations were effective at converting all of the lumens of the tracheids to pixel value equal to 0, however larger rays had pixel values equal to 255. To separate the rays from the resin canals, the aspect ratio of the contours was found. The long rectangular rays were separated from the circular resin canals by converting the contours to pixel value equal to 0 when the ratio of the height to the width was more than 2. The contours with area less than 1600 pixels^2 was converted to pixel value equal to 0 (Figure 7). Three-channel images were saved by merging the contrast fixed and noise removed image with the binary image, and the weighted image which consists of the first two images (Figure 7). There were some errors in the resin canals delineation process, these errors were fixed manually

whereby missing resin canals were added, and any areas that were labeled incorrectly as resin canals were deleted.

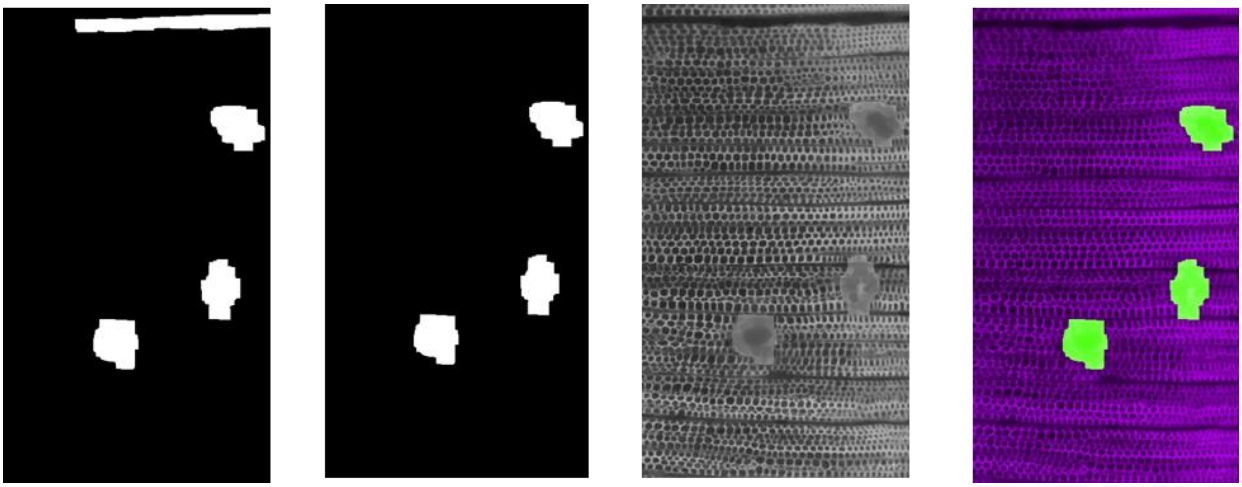

Figure 7: Image sequence from left to right: details eroded and resin complex dilated image, Ray removed image, weighted image, and merged image.

Extracting resin canal information

To extract the resin canals from pith to bark in each sample, the binary images were horizontally concatenated (Figure 8). The contours of the concatenated image were then found. From each contour, the radius, area, perimeter, coordinates for the centroid, maximum and minimum point was calculated using image moments (Teague 1980, Kotoulas and Andreadis 2005). The extracted information, thus, contained sample ID, area in pixels, coordinates (centroid, minimum, maximum) for the x-axis and y-axis for each resin canals. The resin canal information was exported to a comma separated values (CSV) file.

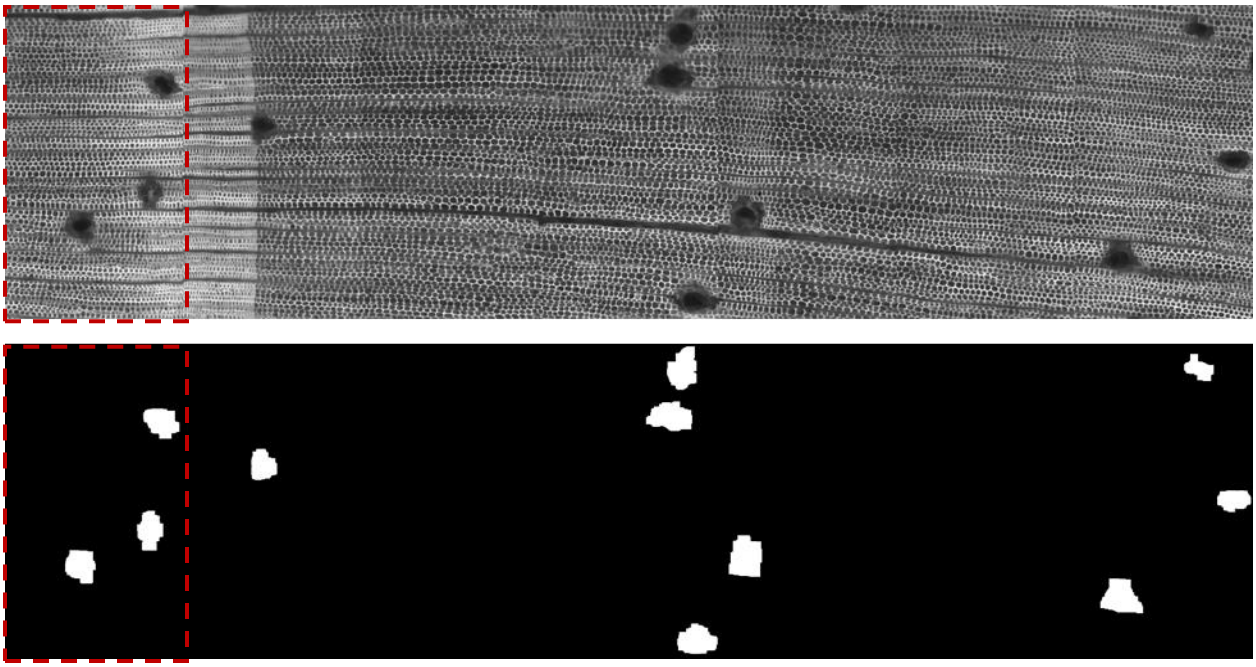

Figure 8: Image subsample showing seven concatenated original image (upper) and contour images (lower).

Merging resin canal data with X-ray densitometry data

The resin canal information was aligned with X-ray densitometry data to assign each resin canal into earlywood and latewood of their respective annual rings. To correct for minor positioning errors between the images and the X-ray data, a pseudo-density value was calculated from the contrast corrected and noise removed images (Figure 8 upper one) by averaging the pixel values of each column of the images (y-axis representing the tangential direction). Because each pixel of the image represents a higher resolution (0.0015 mm) than each X-ray data point (0.04 mm), the image data was averaged in 0.04 mm increments. The pseudo density values were then normalized by:

$$P_D = \frac{x_p - \mu_p}{\sigma_p} \quad (4)$$

where P_D is the normalized pseudo density value (ranging from -1 to 1), x_p is mean pixel value of each column, μ_p is overall means pixel values of each columns means, σ_p is standard deviation of

each column mean. The measured density values from the x-ray densitometer were also normalized by the same procedure. The normalized values from the images and the X-ray densitometer were then aligned using the normalized cross-correlation method (Keane and Adrian 1992, Yoo and Han 2009). The resin canals data were then merged with the X-ray densitometry data in R (R Core Team 2021). Ring level resin canal information was then calculated and included the number, area, average size (area divided by number), and resin canal percent (resin canal area divided by sample area of each ring); the same information was found for the earlywood and latewood proportion of each ring. Incomplete resin canal found at the edge of the samples were counted as half resin canal throughout the calculation process. For example, irrespective of size, if any portion was missing, it was counted as a half resin canal.

2.3. Data Analyses

The statistical analysis and graphics were done using R (R Core Team 2021) and the RStudio interface (RStudio 2020). The libraries used in R include dplyr (Wickham et al. 2018), nlme (Pinheiro et al. 2021), gridExtra (Auguie and Antonov 2017), and ggplot 2 (Wickham et al. 2016). The data generated during this study were assigned at 3 treatment levels, asymptomatic healthy (AH), symptomatic healthy (SH), and symptomatic unhealthy (SU), to compare wood and fiber properties among them. Except for significant values, the line in the graphs are plotted by smoothening particular values at each treatment level using locally weighted smoothing (LOESS) smoothers (span =0.65) (Austin and Steyerberg 2014).

Trees whole core properties

An analysis of variance (ANOVA) using a linear mixed effects model with tree nested in stands was used to compare whole core SG and MC of loblolly pine. Letting Y_{ijk} denote the

value of response variable (SG and MC) for the *i*th tree health, *j*th stand, and *k*th trees, the linear model is:

$$Y_{ijk} = \mu + \alpha_i + \beta_{ij} + \epsilon_{ijk} \quad (5)$$

$$\beta_{ij} \sim N(0, \sigma_\beta) \ and \ \epsilon_{ijk} \sim N(0, \sigma)$$

where, μ is overall mean, α_i is the effect of the *i*th treatments, β_{ij} is the random effect of the *j*th stand having *i*th tree health with $\beta_{ij} \sim N(0, \sigma_\beta)$, ϵ_{ijk} is the effects of the ith tree health, *j*th stand, and *k*th trees with $\epsilon_{ijk} \sim N(0, \sigma)$. The tests were carried out at 0.05 significance level.

Tree ring level properties

The ring level properties were modeled by using a logistic function (Jordan et al. 2008, Antony et al. 2011, Dahlen et al. 2018). The parameters of each function/model were assigned at three treatment levels to test their statistical significance. The models were compared using diagnostic plots, root mean square error (RMSE), log likelihood ratio tests, Akaike information criterion (AIC), and Bayesian Information Criteria (BIC) values.

Specific gravity and acoustic velocity

The four-parameter logistic function having mixed effects factors were used to model and compare both ring level SG and USV. Let Y_{ijk} denote the mean SG or AV of each annual growth ring then the model for ring SG and AV is:

$$Y_{ijk} = \beta_0 + \frac{\beta_1 + b_{1i} + b_{1ij} - \beta_0}{1 + e^{\frac{\beta_2 - CA_{ijk}}{\beta_3}}} \quad (6)$$

where CA_{ijk} is the cambial age of the *k*th annual ring of *j*th tree from *i*th stand, β_0 is the model intercept, β_1 is the model asymptote, β_2 is the inflection point, and β_3 is the scale parameter. Here

parameter β_0, β_1, β_2, and β_3 are fixed effect parameters whereas b_{1i} and b_{1ij} are the nested random effect parameter for the asymptote (β_1) at site and tree level, respectively (Antony et al. 2011, Dahlen et al. 2018).

Latewood specific gravity

To model and compare latewood specific gravity, a three-parameter logistic function with mixed effects in the asymptote was used. Let Y_{ijk} denote the mean latewood specific gravity of each annual growth ring then the model for latewood specific gravity is:

$$Y_{ijk} = \frac{\beta_1 + b_{1i} + b_{1ij}}{1 + e^{\frac{\beta_2 - CA_{ijk}}{\beta_3}}} \quad (7)$$

where CA_{ijk} is the cambial age of the *k*th annual ring of *j*th tree from *i*th stand stand, β_1 is the model asymptote, β_2 is the inflection point, and β_3 is the scale parameter. Here parameter β_1, β_2, and β_3 are fixed effect parameters whereas b_{1i} and b_{1ij} are the nested random effect parameter for the asymptote (β_1) at site and tree level, respectively (Dahlen et al. 2018)

Earlywood specific gravity

The earlywood specific gravity is modeled and compare by using a two-parameter logistic function with mixed effects factors at the intercept. Let Y_{ijk} denote the mean latewood specific gravity of each annual growth ring then the model for earlywood specific gravity is:

$$Y_{ijk} = (\beta_0 + b_{0i} + b_{0ij}) * e^{\frac{\beta_1}{(\beta_2 - CA_{ijk})}} \quad (8)$$

where CA_{ijk} is the cambial age of the kth annual ring of jth tree from ith stand, β_0 is the model intercept, β_1 is the model asymptote, β_2 is the inflection point. Here parameter β_0, β_1, and β_2, are fixed effect parameters whereas b_{0i} and b_{0ij} are the nested random effect parameter for the intercept (β_0) at site and tree level, respectively (Dahlen et al. 2018).

Resin canal area and average size

The resin canal area and size were compared using the 3 parameters logistic function as mentioned in equation (7). The scale parameter (β_3) was varied randomly during modeling the resin canal area and size.

3. Results

3.1 Whole core properties

The whole core SG of the overall stands ranged from 0.38 to 0.63 having an average of 0.48 with SD 0.036. The average SG for asymptomatic healthy trees (0.491, SD = 0.038) was slightly higher than symptomatic healthy (0.480, SD = 0.034) and symptomatic unhealthy (0.475, SD = 0.0332) (Figure 9); however, there is no statistical significance difference for the different treatment levels ($p = 0.273$ for symptomatic healthy and $p = 0.120$ for symptomatic unhealthy).

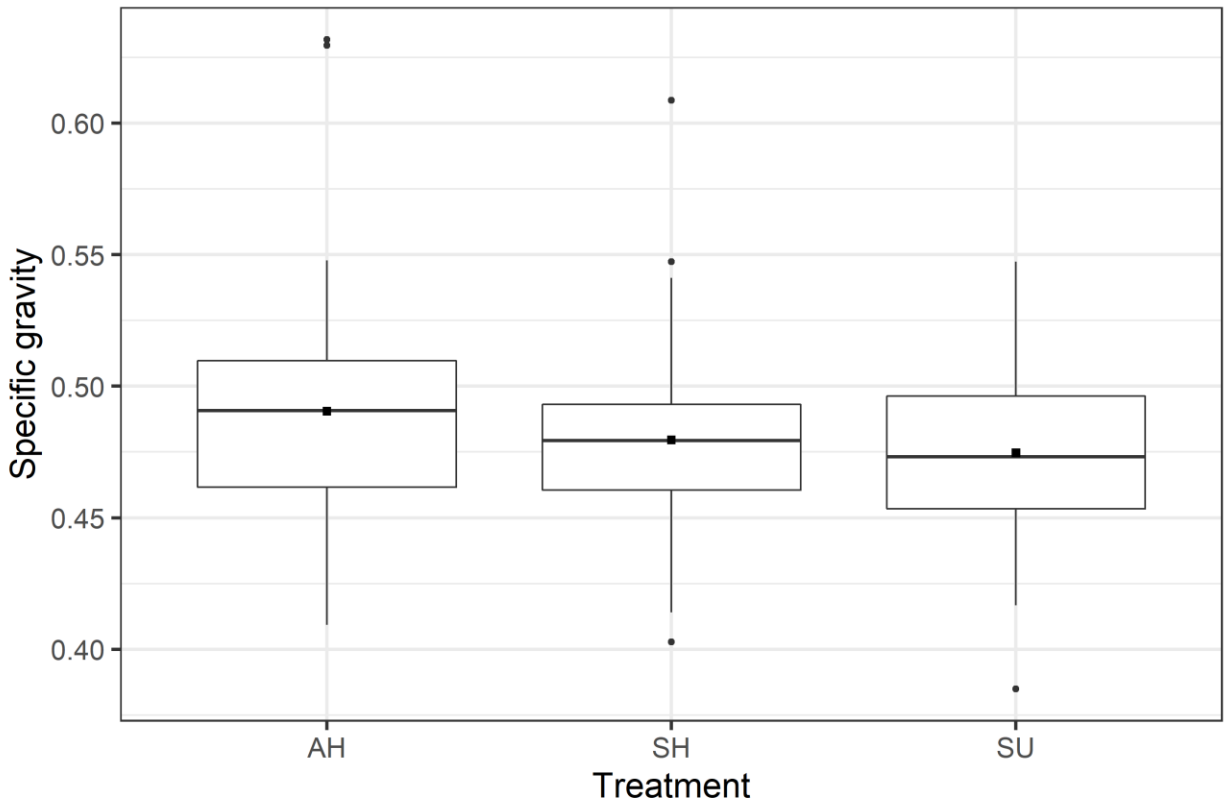

Figure 9: Whole-core specific gravity for each treatment level. The small square at the center of boxplot indicates the average and the line indicates median specific gravity.

The overall average MC was 84.72% (SD = 16.028) and ranged from 40.49% to 134.56%. Unlike SG, the average MC (%) of symptomatic unhealthy tees (87.2%, SD = 17.6%) is slightly higher than symptomatic healthy (84.4, SD = 16.2) and asymptomatic healthy trees (82.2, SD = 13.8) (Figure 10). But there was no difference in MC (%) among the treatments (p= 0.485 for symptomatic healthy and p= 0.105 for symptomatic unhealthy trees).

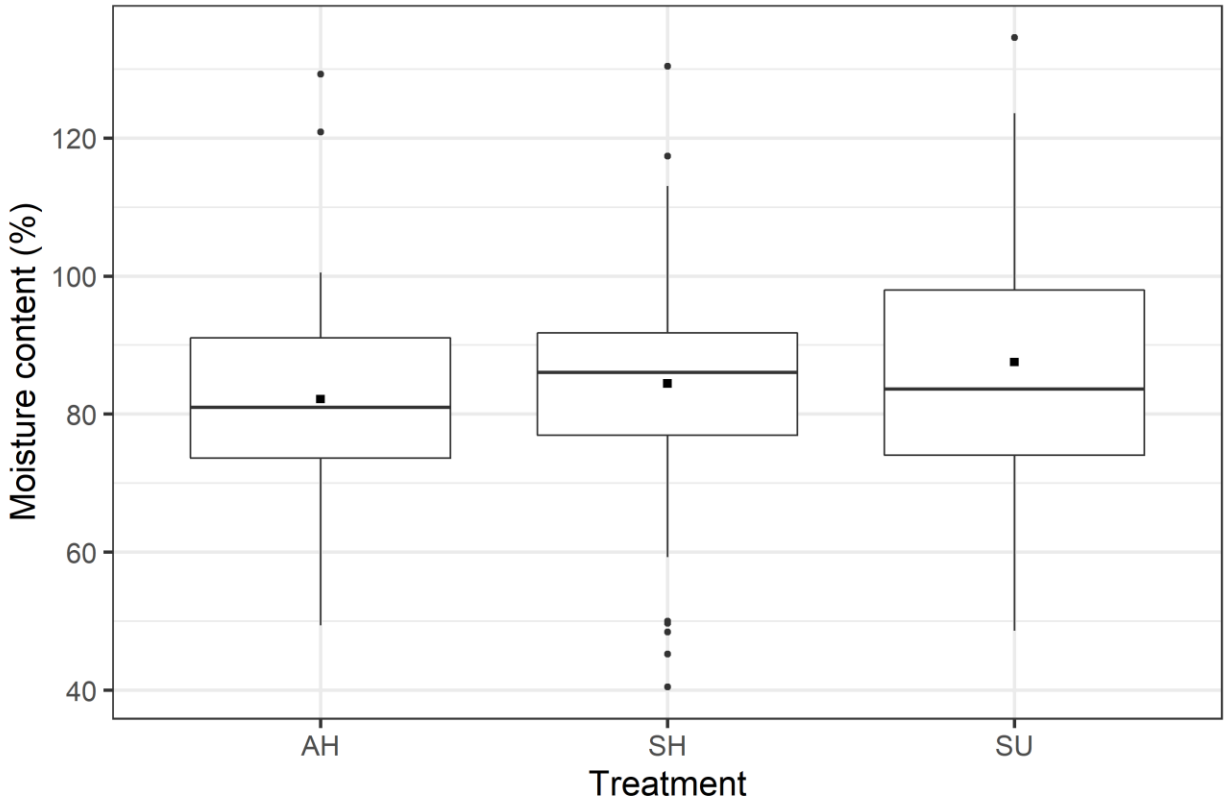

Figure 10: Boxplot showing moisture content (%) of the trees at each treatment level. Small square at the center of boxplot indicates the average value of moisture content and line indicates the median of moisture content (%).

3.2 Ring level properties

Cambial age

The cambial age of the trees represents the ring number count in the samples. The overall cambial age of trees at each treatment level is similar having the similar minimum and maximum age (Table 3).

Table 3: Cambial age at DBH by treatment

Treatments	Cambial age at breast height (years)			
	Mean	SD	Min	Max
Asymptomatic Healthy (AH)	22	3.3	17	28
Symptomatic Healthy (SH)	21.4	3.26	17	28
Symptomatic unhealthy (SU)	21	3.36	15	28

Growth over time - ring width and basal area

The average tree ring width is higher for symptomatic healthy trees (5.68 mm, SD = 3.31), followed by asymptomatic healthy trees (5.61 mm, SD = 3.06) and symptomatic unhealthy trees (5.25, SD = 3.32). At young cambial ages, the trees have larger ring widths and as the tree ages the ring width decreases (Figure 11). The symptomatic unhealthy trees have slightly narrower ring widths than symptomatic healthy trees after approximately 10 years.

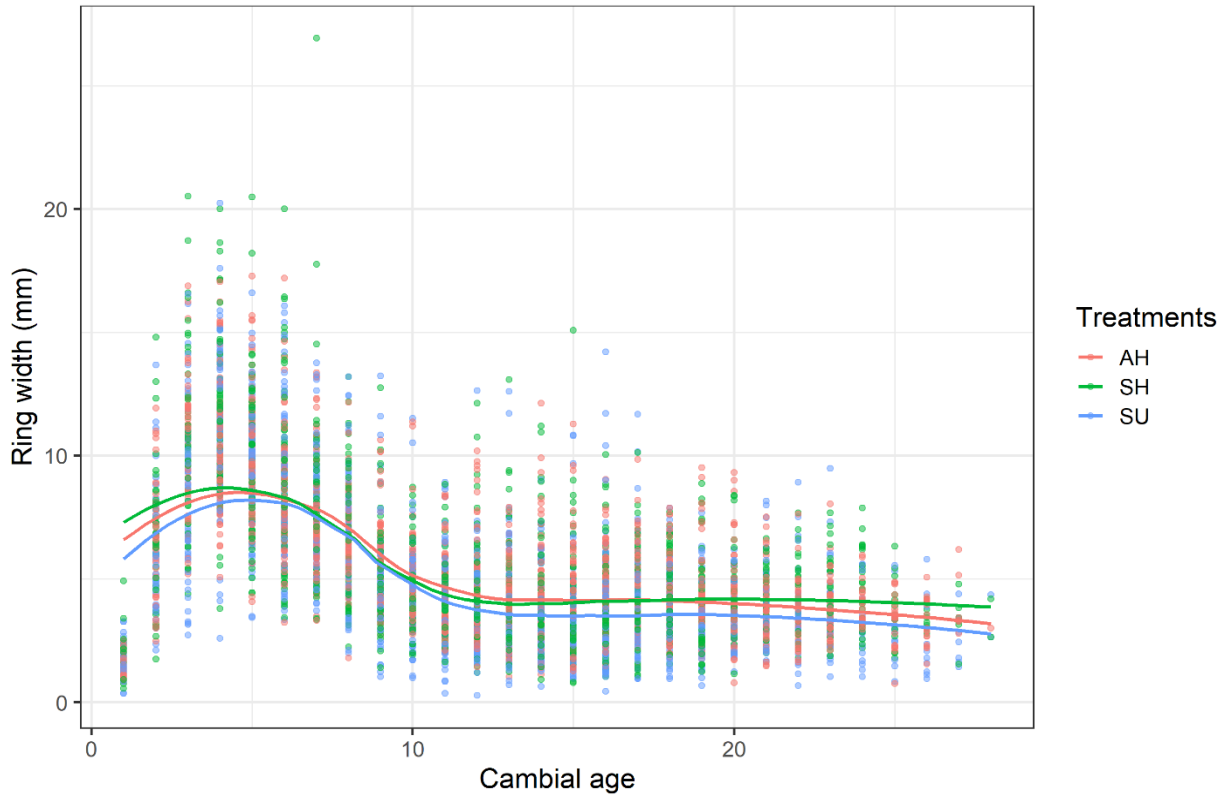

Figure 11: Ring width of the samples along the radius of the trees

Unlike ring width, the ring basal area gradually increases with the age of the trees (Figure 12). At treatment levels, symptomatic unhealthy trees have a lower ring basal area (19.3 cm^{-3}, SD = 13.9) than the symptomatic healthy trees (22.5 cm^{-3}, SD =14.5) with the asymptomatic healthy trees

being in the middle (22.7 cm^{-3}, SD = 12.7). At cambial age 9-14 years, the trees show a pattern of declining growth which might be due to competition occurring prior to thinning.

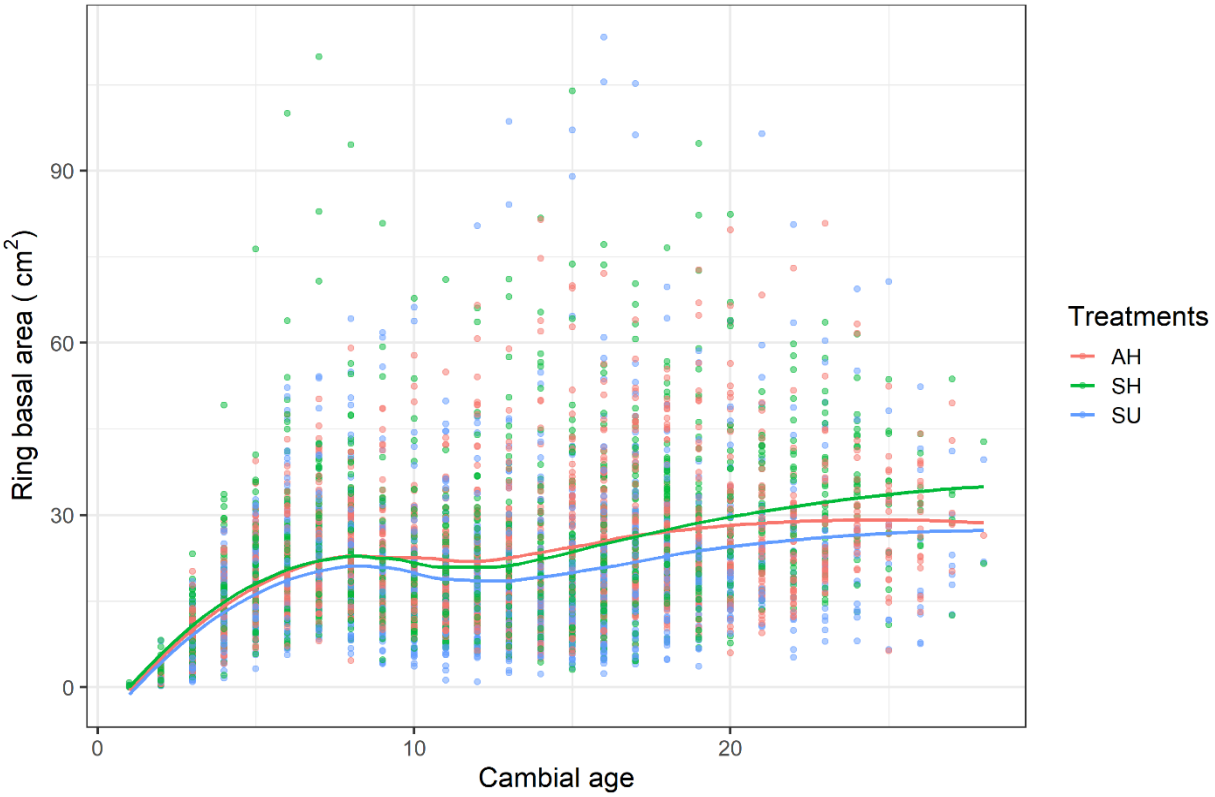

Figure12: Ring basal area of the sampled trees versus cambial age.

Specific gravity and acoustic velocity

Overall descriptions

Overall ring specific gravity for the 14 stands is 0.482 (SD = 0.076), latewood percent is 42.9% (SD = 18.39), and acoustic velocity is 4,322 ms^{-1} (SD = 606). At trees levels (averaged rings levels values to get one value for one tree), the average ring SG and AV were almost similar; however, there is a significant difference in average earlywood SG (p = 0.030) between asymptomatic healthy and symptomatic unhealthy (Table 4). Unlike earlywood SG, there was no significant difference in latewood specific gravity among treatment groups at trees levels (for

asymptomatic healthy and symptomatic unhealthy, p = 0.0578). Average earlywood SG was higher in symptomatic healthy trees (0.319), followed by symptomatic unhealthy trees (0.324) and asymptomatic healthy trees (0.319). The reverse was true for latewood SG where average latewood specific gravity is higher in asymptomatic healthy trees (0.684) followed by symptomatic healthy trees (0.674) and symptomatic unhealthy trees (0.665).

Table 4. Summary of ring, earlywood, and latewood specific gravity, latewood percent, and acoustic velocity (m/s).

Treatments	**Specific gravity**			**Latewood (%)**	**Acoustic Velocity**
	Ring	**Earlywood***	**Latewood**		
Asymptomatic healthy (AH)	0.486(0.076)	0.319(0.031) a	0.684(0.075)	43(17.7)	4337(614)
Symptomatic healthy (SH)	0.480(0.074)	0.324(0.029) ab	0.674(0.069)	42(17.8)	4356(602)
Symptomatic unhealthy (SU)	0.481(0.078)	0.328(0.033) b	0.665(0.071)	43(19.7)	4274(602)

* indicates significant differences. Different letters indicate significant differences ($p<0.05$)

Acoustic velocity (AV)

Acoustic velocity increased from pith to bark (Figure 13). The average AV at cambial age 1 was 3407 m/s whereas maximum average AV at 28 years was 4844 m/s. There is not any noticeable difference of AV among the treatment groups.

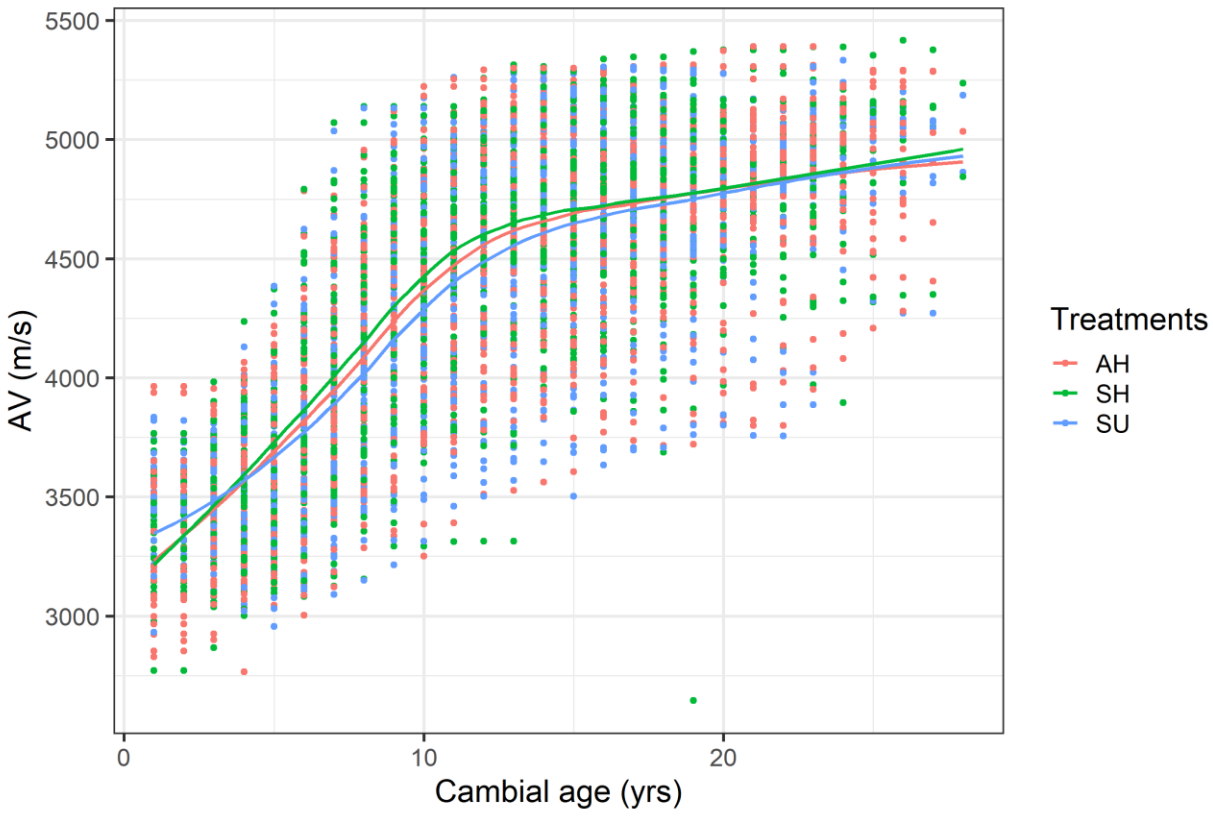

Figure 13: Acoustic velocity (AV) of the samples along the cambial age.

Ring specific gravity

Like AV, the ring specific gravity also increased with increases in cambial age (Figure 14). Looking at treatment differences, the intercept (cambial age = 1) and inflection point of the curve was almost similar. There were some minor differences between the asymptote value between treatments, however the differences were not significant ($p = 0.2431$ for symptomatic healthy and $p = 0.0879$ for symptomatic unhealthy).

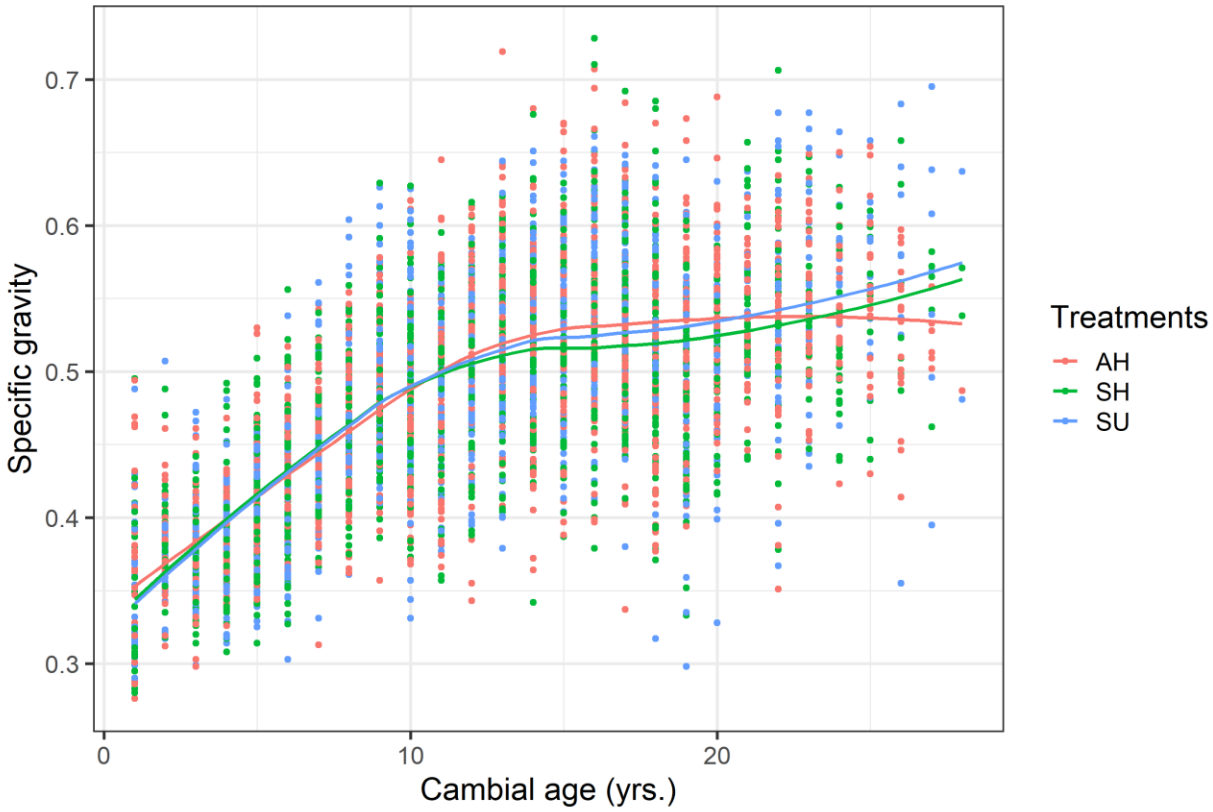

Figure 14: Ring specific gravity of the sample versus cambial age.

Latewood percentage

Latewood percent followed a similar pattern as ring specific gravity. With increases in cambial age the latewood percent also increased (Figure 15). There were not any differences among the treatment groups.

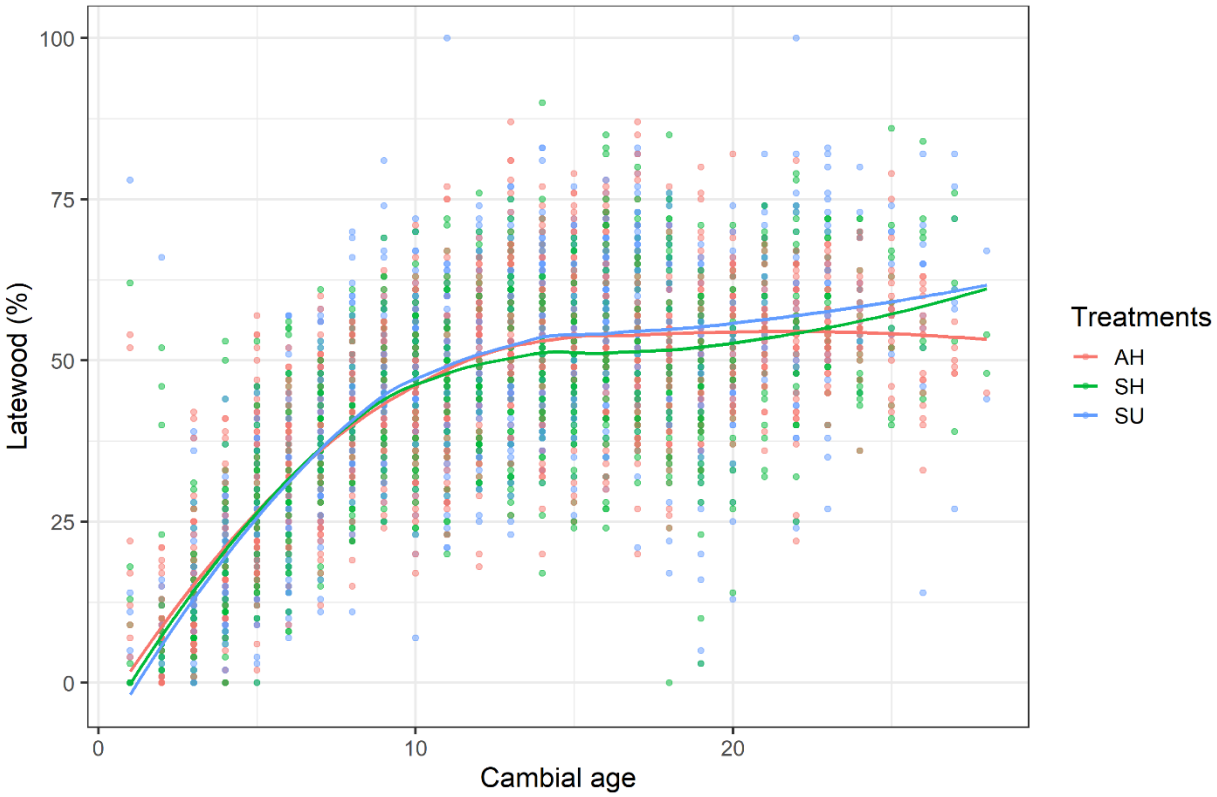

Figure 15: Latewood (%) of the samples along the radius of the trees

Latewood specific gravity

Latewood specific gravity increases with cambial age (Figure 16). There was a significant difference between treatments for the latewood specific gravity model and the parameters values and fit indices reported in Table 5. Significant differences among the treatment groups in the asymptote and scale parameters were found. The asymptomatic healthy treatment has a higher latewood SG asymptote value than the other treatments, and the symptomatic unhealthy trees have the lowest latewood SG asymptote value ($p = 0.0006$). Likewise, there was a significant difference in the scale parameter (rate parameter) for the asymptomatic healthy trees compared to the symptomatic healthy ($p = 0.0013$) and symptomatic unhealthy trees ($p = 0.0013$).

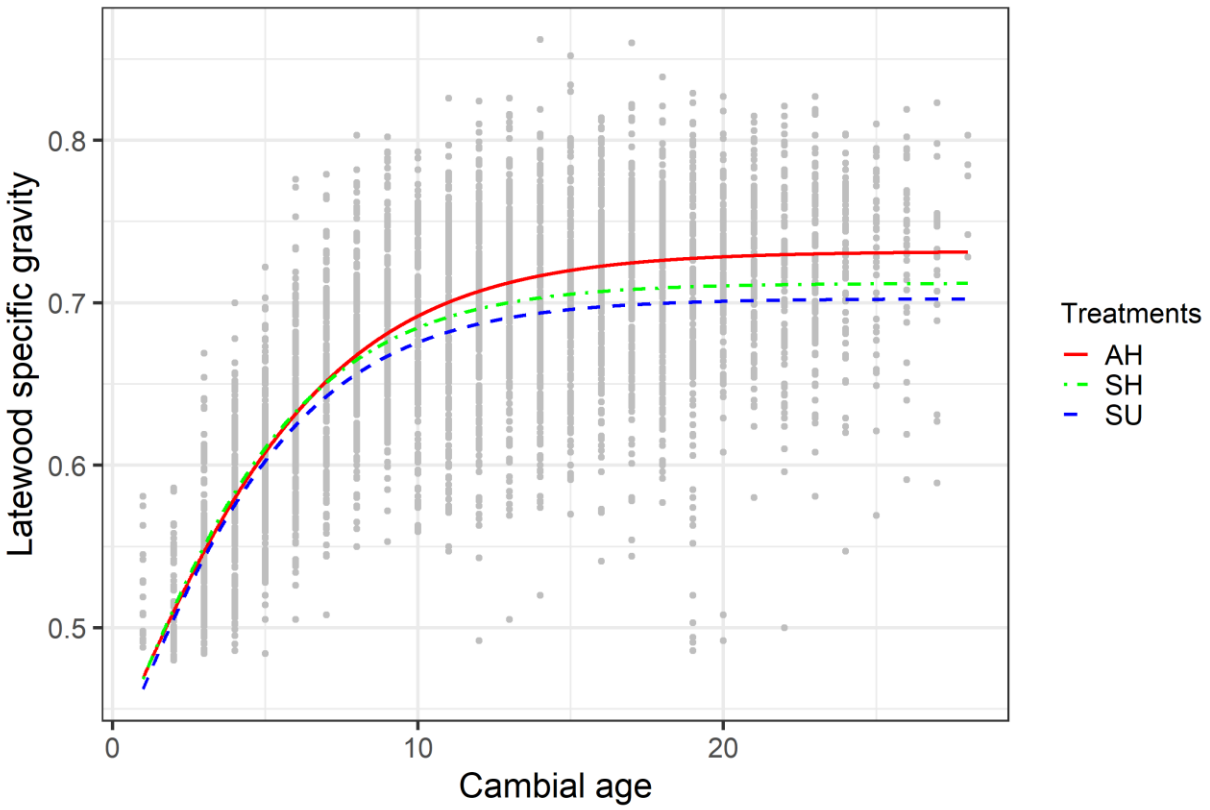

Figure 16: Predicted and measured latewood specific gravity versus cambial age for the 3 treatments.

Table 5: The parameters value and fit indices for the latewood specific gravity.

Parameters	**Value**	**Standard error**	**p-value**
β_1 (asymptomatic healthy)	0.7316	0.0061	0.0000
β_1 (symptomatic healthy)	-0.0196	0.0085	0.0214
β_1 (symptomatic unhealthy)	-0.0291	0.0085	0.0006
β_2	-1.2940	0.1649	0.0000
β_3 (asymptomatic healthy)	3.9528	0.1557	0.0000
β_3 (symptomatic healthy)	-0.4457	0.1384	0.0013
β_3 (symptomatic unhealthy)	-0.4523	0.1402	0.0013

Fit indices and error statics

AIC	**Fit Indices (R2)**			**Model Errors**		
	Fixed	**Site**	**Tree**	**E**	**RMSE**	**|E|%**
-14352	0.5148	0.5405	0.6786	0.0005	0.0503	5.9400

Earlywood specific gravity

Earlywood specific gravity decreases with increased cambial age (Figure 17). There was a significant difference between treatments for the earlywood specific gravity model and the parameters values and fit indices reported in Table 6. The symptomatic unhealthy trees had the highest earlywood SG asymptote values, with the asymptotic healthy treatment having the lowest value ($p < 0.001$). There was a significant difference in the inflection point between the asymptomatic healthy and the symptomatic unhealthy trees ($p = 0.002$). Also, there was significant difference in the asymptote ($p = 0.036$) and infection point ($p = 0.029$) between symptomatic healthy and symptomatic unhealthy trees.

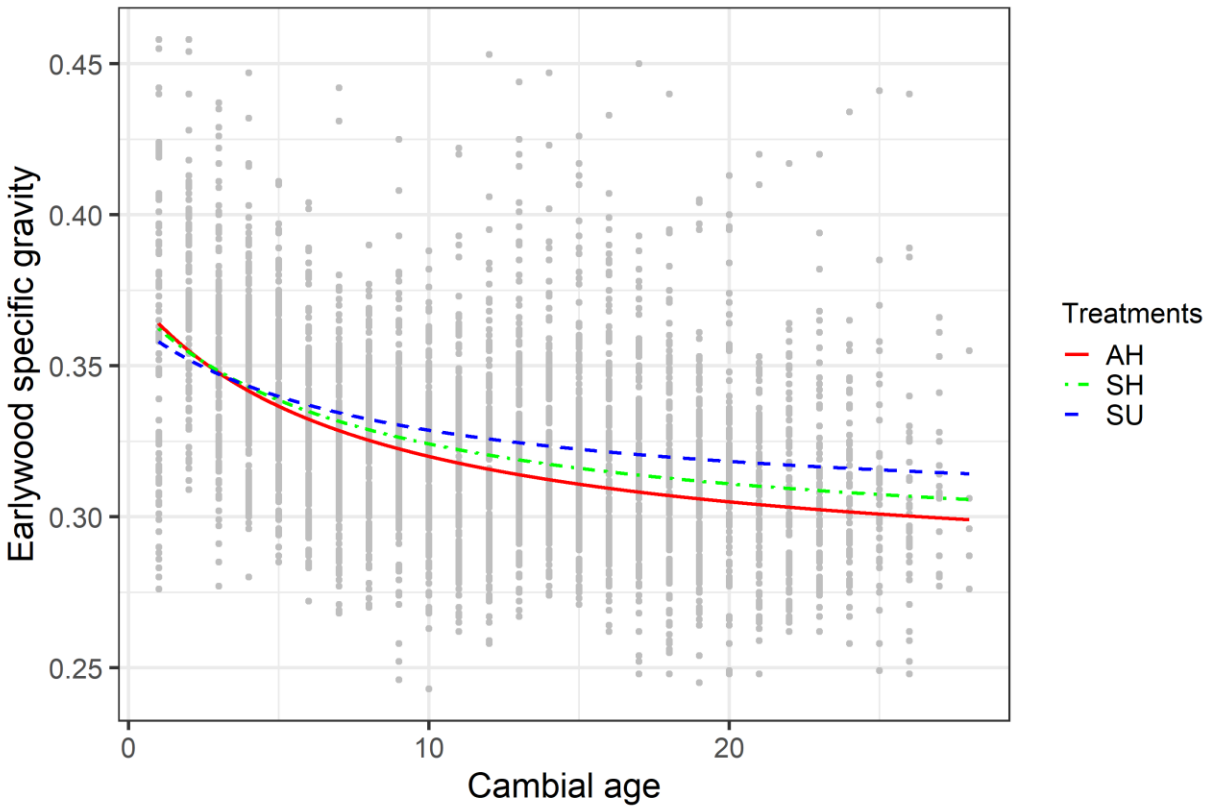

Figure 17: Predicted and measured earlywood specific gravity versus cambial age for the 3 treatments.

Table 6: The parameters and fit indices for the earlywood specific gravity.

Parameters	Value	Standard error	p-value
β_1 (asymptomatic healthy)	0.2787	0.0054	0.0000
β_1 (symptomatic healthy)	0.0090	0.0044	0.0394
β_1 (symptomatic unhealthy)	0.0212	0.0045	0.0000
β_2 (asymptomatic healthy)	2.5744	0.5944	0.0000
β_2 (symptomatic healthy)	-0.3502	0.2246	0.1191
β_2 (symptomatic unhealthy)	-0.8686	0.2815	0.0020
β_3	8.6469	1.7703	0.0000

Fit indices and error statics

AIC	Fit Indices (R2)			Model Errors		
	Fixed	Site	Tree	E	RMSE	|E|%
-19633	0.1823	0.2009	0.4221	-0.0002	0.0279	6.5539

Resin canals

Overall description

A total of 24,865 resin canals having a total area of 750 mm^2 from 24,153 images were imaged from 210 samples. Overall asymptomatic healthy trees have more resin canals (8,800) and higher area (273 mm^2) than the symptomatic healthy trees (8,013, area = 245 mm^2) and symptomatic unhealthy trees (8,052, area = 232 mm^2) (Table 7). The average size of resin canals is larger for the asymptomatic healthy trees (0.0356 mm) than symptomatic unhealthy trees (0.0323 mm) and symptomatic healthy trees are intermediate (0.0347 mm). Additionally, the percent of resin canal area to ring area is higher for asymptomatic healthy trees followed by symptomatic unhealthy trees and symptomatic healthy trees (Table 7).

Table 7: Resin canal summary within the area imaged.

Treatments	**Resin canals**			
	Number	**% of ring**	**Total area (mm^2)**	**Average size (mm^2)**
Asymptomatic Healthy (AH)	8800	1.82	272.79	0.0356(0.013)
Symptomatic Healthy (SH)	8013	1.66	245.12	0.0347(0.012)
Symptomatic Unhealthy (SU)	8052	1.76	231.51	0.0323(0.011)

Note: Data were not statistically different at trees levels.

Overall resin canal number and area in earlywood and latewood wood

We found more resin canals in the earlywood than the latewood. From Table 4, the average amount of latewood was 43%, and we also found that 43% of the resin canals were within the latewood (Table 4 and Table 7). Thus, the resin canals are about equally formed in the earlywood and the latewood. A similar pattern of latewood and earlywood resin canals numbers and area were found among the treatment groups (Table 8).

Table 8: Resin canal summary found in earlywood versus latewood using a 0.48 specific gravity threshold.

Treatments	Resin Canals							
	Total		Earlywood			Latewood		
	N	Area (mm^2)	N	%N	Area (mm^2)	N	%N	Area (mm^2)
AH	8800	273	4901	55.7	136	3900	44.3	137
SH	8013	245	4406	55.0	118	3606	45.0	127
SU	8052	232	4544	56.4	114	3508	43.6	117

Overall, earlywood, and latewood resin canal number by cambial age

Overall, resin canals numbers followed the trend of ring width with resin canal number decreasing with increases in cambial age (Figure 18). The reduction in the number of resin canals imaged was pronounced through up to 10 years and then decreased slightly after 10 years. There was no apparent difference in resin canals numbers among treatments.

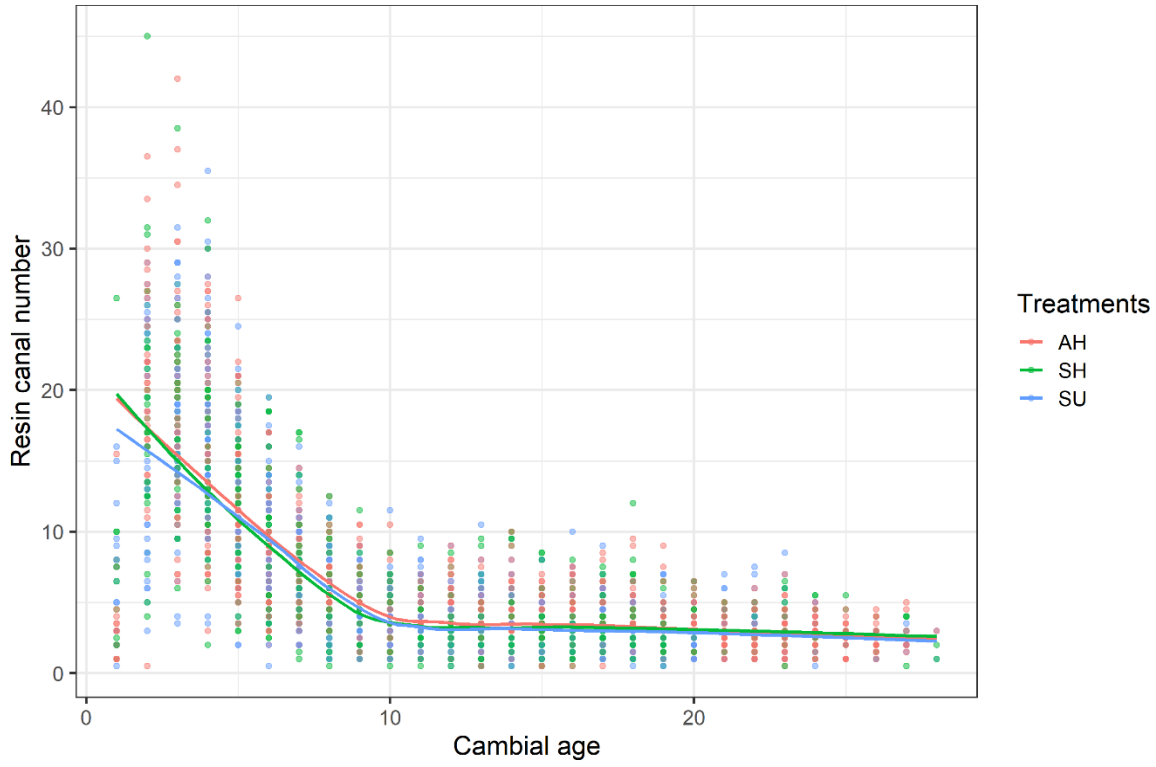

Figure 18: Number of resin canals in each ring versus cambial age

Earlywood resin canals numbers also followed the similar pattern of overall resin canal numbers and ring width (Figure 19). There was no apparent difference among the treatment groups.

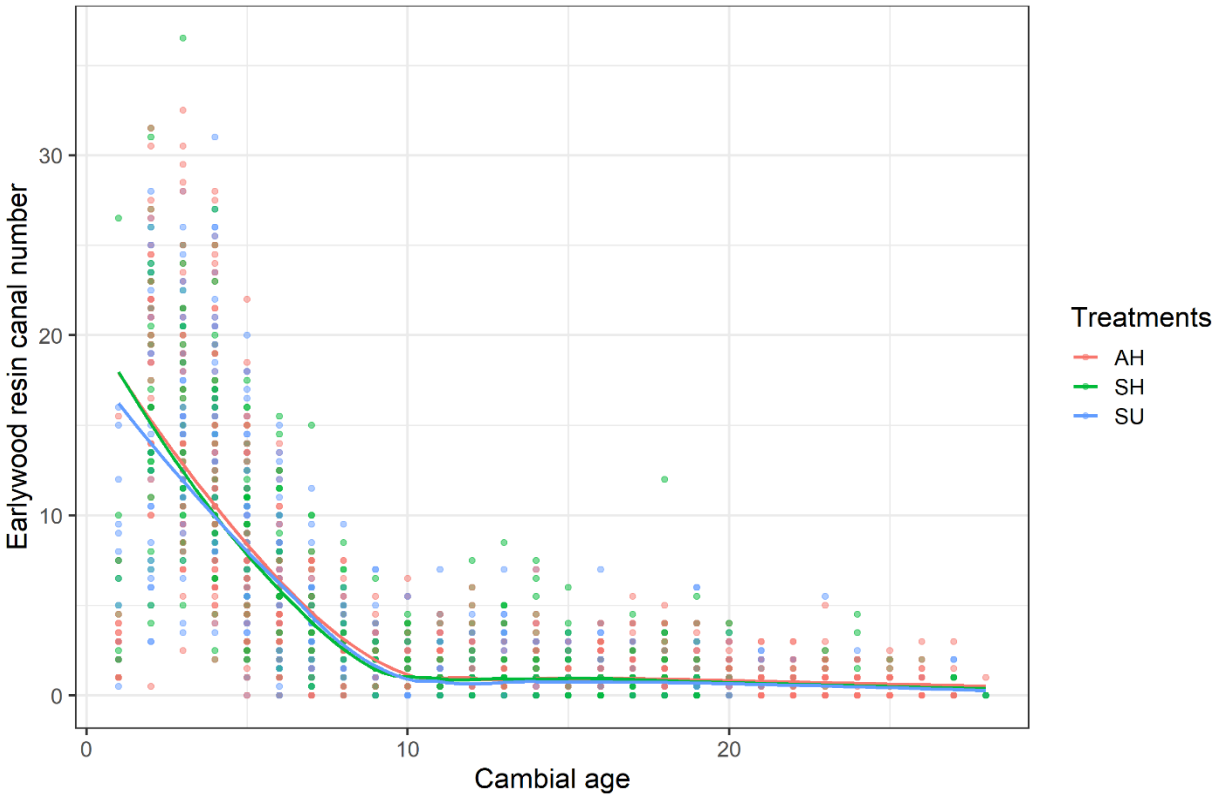

Figure 19: Number of resin canals in the earlywood versus cambial age.

Unlike earlywood, latewood resin canals number showed an increasing pattern up to cambial age 7 years then slightly decreased until 10 years and remained steady after then (Figure 20). There was no apparent difference in the number of resin canals found in the latewood by treatment by cambial age.

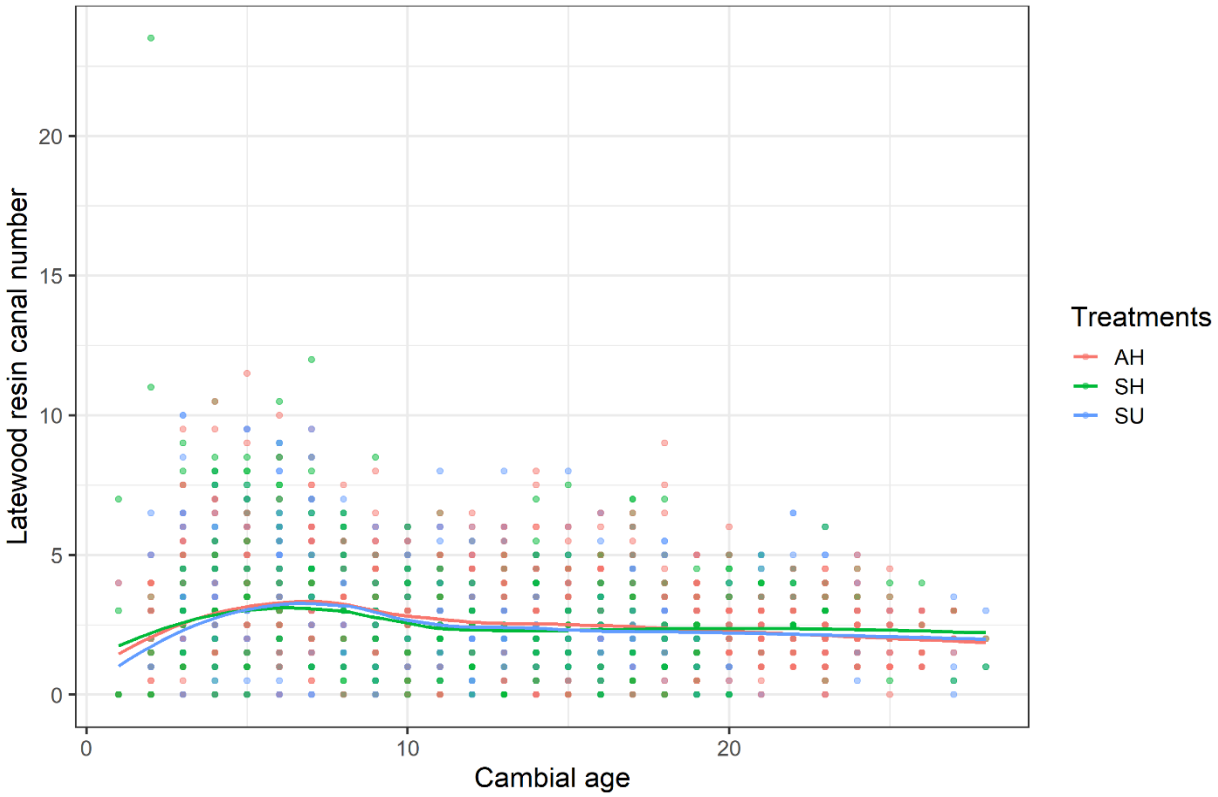

Figure 20: Number of resin canals in the latewood versus cambial age.

Resin canal area by cambial age

The overall trend of resin canal area follows the ring width trend with some observed treatment differences (Figure 21). The asymptomatic healthy trees have a higher resin canal area than symptomatic unhealthy trees; the symptomatic healthy trees are between the asymptomatic healthy and symptomatic unhealthy trees.

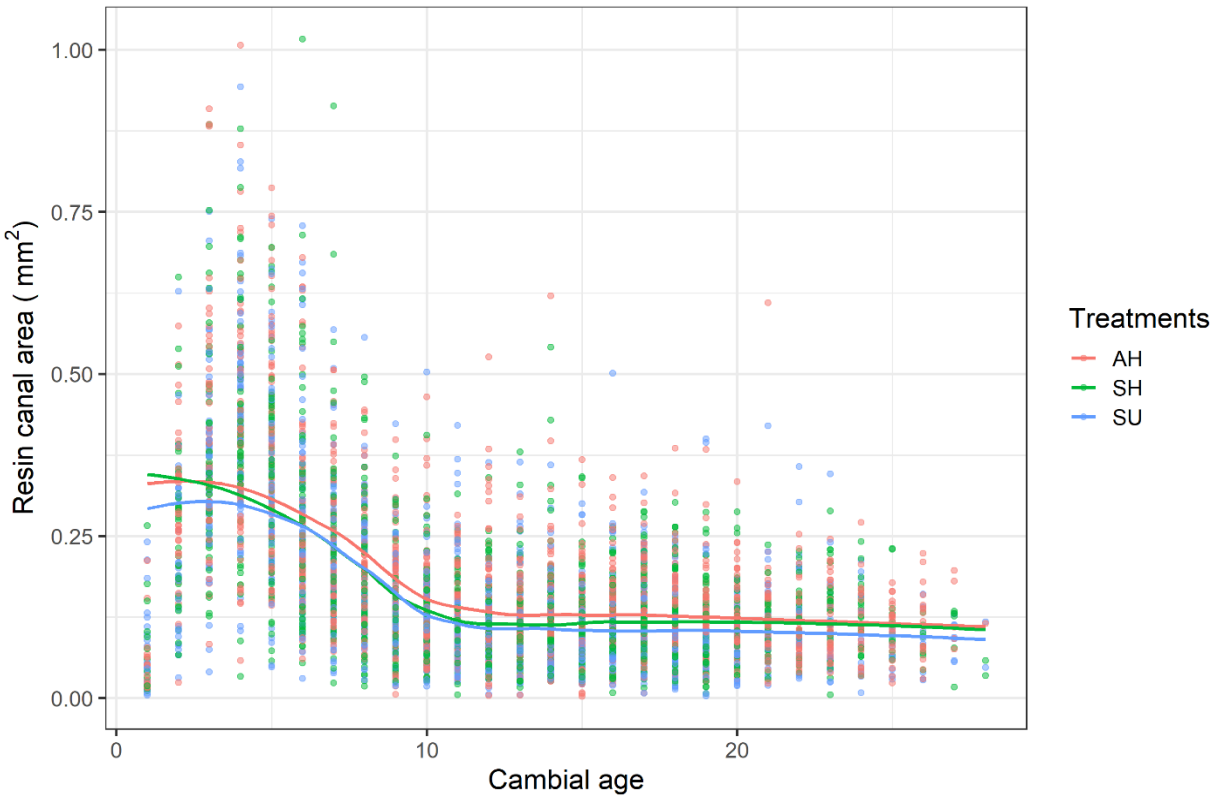

Figure 21: Resin canal area of the sample along with cambial age (imaged portion only).

The resin canal area (%) decreases for approximately 9 years, after that there is a slight increase in area percent for the asymptomatic healthy trees (Figure 22). The symptomatic unhealthy trees is between the asymptomatic healthy and symptomatic healthy treatments.

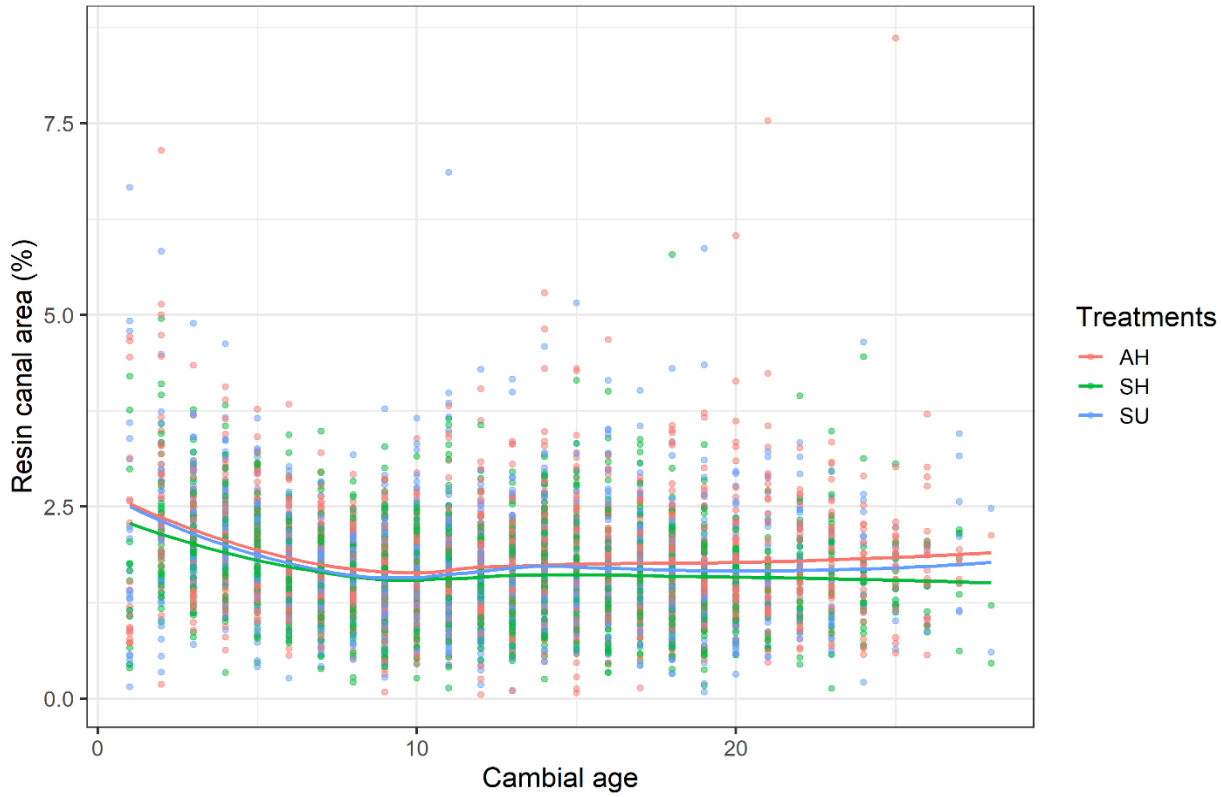

Figure 22: Percent of resin canal area to ring area (imaged portion only).

The resin canal basal area within the sample is interpolated based on the ring basal area of the trees. The trend follows a similar trend as the ring basal area of the trees. The asymptomatic healthy trees have a larger resin canal basal area than that of symptomatic unhealthy trees (Figure 23).

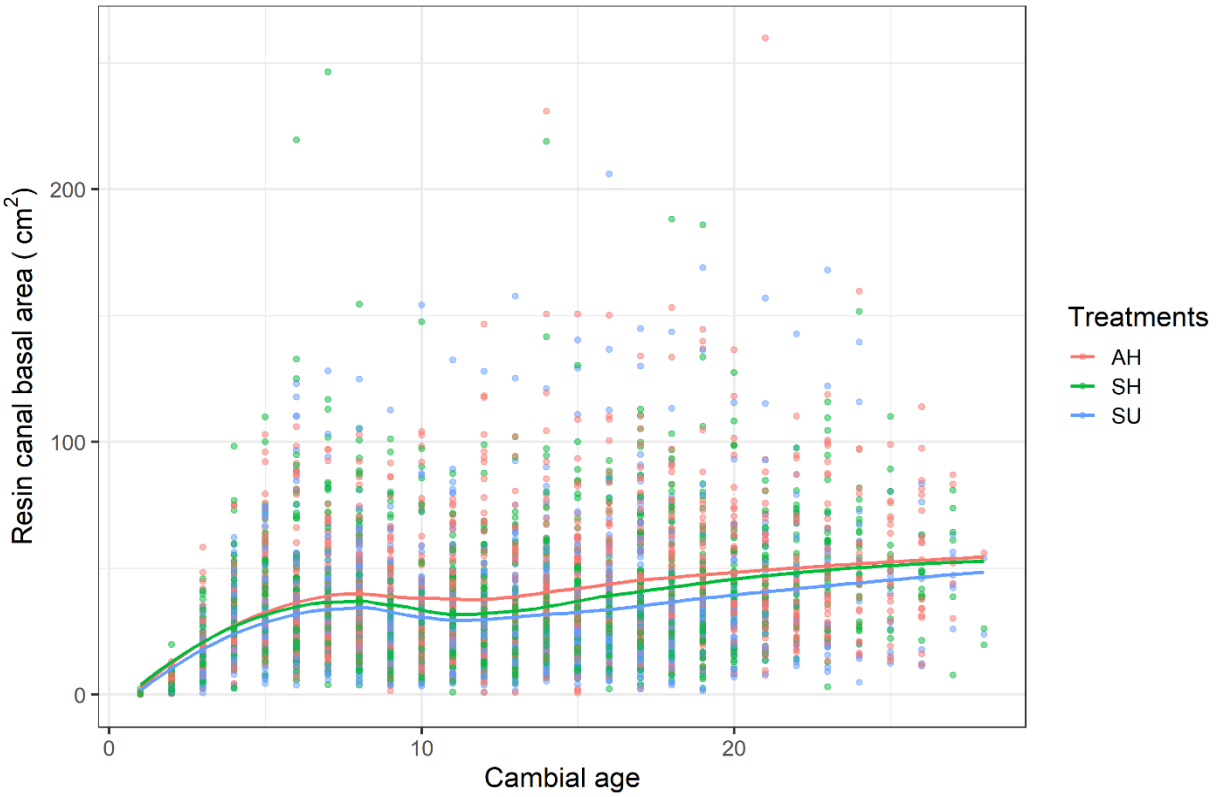

Figure 23: Resin canals basal area interpolated to ring basal area

Average size of the resin canals

The average size of resin canals increased with cambial age (Figure 24). As cambial age increased the asymptomatic healthy and symptomatic healthy trees had significantly larger resin canals than the symptomatic unhealthy trees based on the asymptote parameter for the nonlinear model ($p = 0.0000$ and 0.0290). Asymptomatic healthy trees also had significantly larger resin canals than the symptomatic healthy trees with time ($p = 0.0020$) (Table 9). There was significant difference in scale parameter between asymptomatic healthy and symptomatic healthy trees ($p = 0.0369$). Moreover, no differences in scale ($p = 0.5600$) parameters were found between symptomatic healthy and symptomatic unhealthy trees.

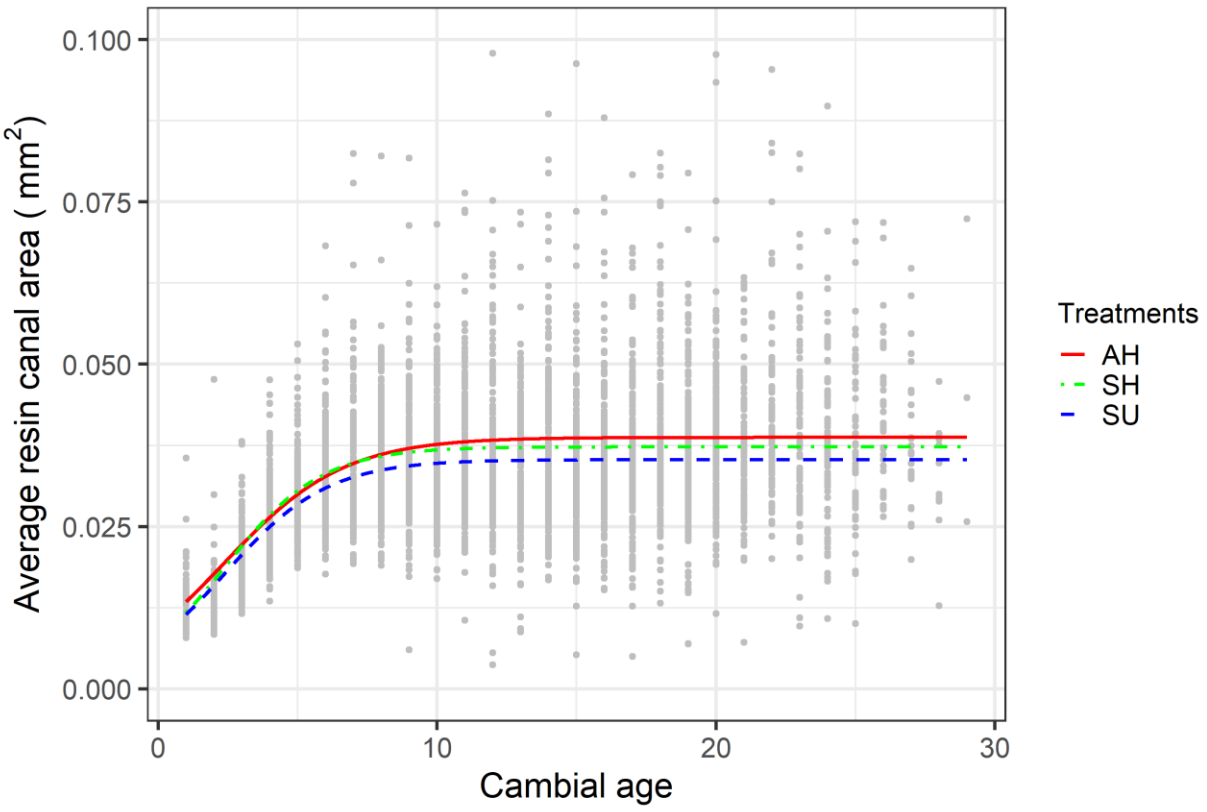

Figure 24: Predicted and measured average size of the resin canals versus cambial age.

Table 9: The parameters and fit indices for the resin canal size.

Parameters	**Value**	**Standard error**	**p-value**
β_1 (asymptomatic healthy) **a**	0.0387	0.0005	0.0000
β_1 (symptomatic healthy) **b**	-0.0015	0.0007	0.0290
β_1 (symptomatic unhealthy) **c**	-0.0034	0.0007	0.0000
β_1 (**b** vs **c**)	-0.0020	0.0007	0.0020
β_2	2.4255	0.0976	0.0000
β_3 (asymptomatic healthy)	2.1448	0.1439	0.0000
β_3 (symptomatic healthy)	-0.3962	0.1898	0.0369
β_3 (symptomatic unhealthy)	-0.2920	0.1936	0.1317

Fit indices and error statics						
AIC	**Fit Indices (R2)**			**Model Errors**		
	Fixed	**Site**	**Tree**	**E**	**RMSE**	**|E|%**
-27441	0.2072	0.2087	0.2163	0.0001	0.0112	21.6969

Note: Letter ‘a’, ‘b’, and ‘c’ in parameters column represent significant difference.

4. Discussion

The symptomatic unhealthy trees had lower ring widths than the healthy trees (Figure 10). The lower ring widths in symptomatic unhealthy trees was ultimately associated with lower tree growth (Table 2). Trees in the symptomatic stands may have been suffering from stress resulting in the production of fewer and smaller diameter tracheids (Lauder et al. 2019). Rossi et al. (2009) found that *Abies balsamea* seedlings produced tracheids with up to a 50% reduction in cell diameter and lumen area during dry periods. The smaller tracheids and fewer number of tracheids leads to production of narrower rings (Wodzicki et al. 1983, Wodzicki 2001, Xu et al. 2014). Bouriaud et al (2005) reported that soil water content is an important parameter for variation in tracheid size in Norway spruce *(Picea abies).* Dalla-Salda et al. (2009) found significant growth reduction in Douglas-fir *(Pseudotsuga menziesii)* during a heat wave and drought.

The symptomatic unhealthy trees had higher earlywood specific gravity than asymptomatic healthy and symptomatic healthy trees. Earlywood specific gravity may increase due to changes in physiological process of trees suffering from external stress (e.g. drought, low nutrients). For example, earlywood specific gravity increases with moisture stress (Hacke et al. 2001) due to the production of narrow diameter tracheids with smaller lumens with thicker cell walls in order to prevent implosion from the high negative tensions (Erickson and Arima 1974, Pittermann et al. 2006a). This results in more energy being invested in the production of the thicker cell which might compromise the growth of the latewood tracheids (Hacke et al. 2001, Pittermann et al. 2006b). Trees experiencing drought in the early growing season might produce false rings which have narrow diameter latewood tracheids (Larson 1963, Campelo et al. 2007). Perhaps the symptomatic unhealthy trees were experiencing moisture stress or drought

throughout their life which also reduced their growth. Latewood SG was lower in symptomatic stands than asymptomatic stands which may also be due to the moisture stress. Trees in late growing season may have less energy to produce enough thicker wall tracheids, as they already invested more energy in the early growing season tracheids (Novaes et al. 2010), which might lead to reduction of latewood specific gravity in the symptomatic stands. Jordan et al. (2008) hypothesized that loblolly pine growing near the southern coasts had higher SG because of a longer growing season and more water available in late summer.

When combining the earlywood and latewood SG results together, the ring SG, latewood % and MC were not significantly different. As there was no significant difference in the ring SG and acoustic velocity, there might be little or no impact on the utilization of the wood from loblolly pine experiencing dieback when used for structural purposes. The change in the earlywood and latewood SG may result in a difference in the amount of lignin deposited in the tracheids which could affect the pulp yield (Smook 2002, Barnett and Jeronimidis 2003).

Traumatic resin canals were absent in both symptomatic and asymptomatic stands. Traumatic resin canals are formed when there is damage in the cambium layer of trees (Lombardero et al. 2000). The symptomatic unhealthy trees we sampled were suffering from stress and not a disturbance event which may be the reason why only constitutive resin canals were produced. No appreciable difference in the number of resin canals number was found, however the average resin canal size was larger in the asymptomatic stands than the symptomatic stands. Within symptomatic stands, the healthy trees produced larger resin canals than unhealthy trees. Larger resin canals are associated with more production, storage and translocation of resin in damaged regions (Franceschi et al 2005, Erbilgin et al 2017, Zhao and Erbilgin 2019). Hood et al (2015) found that ponderosa pine trees that died from beetle attack had smaller axial resin

canals with lower percentage of ring area compared to the trees that survived. Whitebark pine (*Pinus albicaulis*) surviving from mountain pine beetle outbreaks produced larger resin canals and area by 56% and 46%, respectively (Kichas et al 2020). The larger resin canals of asymptomatic healthy trees and symptomatic healthy trees than symptomatic unhealthy trees may lead to their defensive capacity and survival.

The study examined wood anatomical and physical properties of symptomatic and asymptomatic stands. We found significant differences in the earlywood specific gravity, latewood specific gravity, and resin canal size between symptomatic and asymptomatic stands. We hypothesize that the differences might be the due to symptomatic stands suffering from soil moisture or nutrient stress. If pine dieback could be detected early, a future study that examined abiotic factors including soil water content, soil nutrients, and climate along with biotic factors could yield more conclusive results.

5. Conclusions

Whole core and ring level wood properties and resin canals were compared among asymptomatic healthy, symptomatic healthy, and symptomatic unhealthy trees. At the ring level, trees suffering from dieback produced higher SG earlywood and lower SG latewood than healthy trees. We found that trees in asymptomatic stands produced larger resin canals than trees in symptomatic stands, and within symptomatic stands we found that healthy trees produced larger resin canals than unhealthy trees that were suffering from dieback. The production of larger resin canals by the asymptomatic healthy trees were linked with their higher defensive capacity and survival. This study provided novel data and a framework for linking tree health defense responses with wood anatomy, specifically resin canals. This study provides a guide toward the interlinking wood anatomical properties, tree defense systems, and tree hydraulics.

References

Antony, F., Schimleck, L.R., Jordan, L., Clark, A. and Daniels, R.F., 2011. Effect of early age woody and herbaceous competition control on wood properties of loblolly pine. *Forest Ecology and Management*, *262*(8):1639-1647.

Antony, F., Schimleck, L.R. and Daniels, R.F., 2012. Identification of representative sampling heights for specific gravity and moisture content in plantation-grown loblolly pine (Pinus taeda). *Canadian Journal of Forest Research*, *42*(3):574-584.

ASTM D2395-17., 2017. Standard Test Methods for Density and Specific Gravity (Relative Density) of Wood and Wood-Based Materials, ASTM International, West Conshohocken, PA, 2017, www.astm.org

ASTM D4442-20., 2020. Standard Test Methods for Direct Moisture Content Measurement of Wood and Wood-Based Materials, ASTM International, West Conshohocken, PA, www.astm.org

Auguie, B., Antonov, A. and Auguie, M.B., 2017. Package 'gridExtra'. *Miscellaneous Functions for "Grid" Graphics*.

Austin, P.C. and Steyerberg, E.W., 2014. Graphical assessment of internal and external calibration of logistic regression models by using loess smoothers. *Statistics in medicine*, *33*(3):517-535.

Ayres, M.P., 1993. Plant defense, herbivory, and climate change. *Biotic interactions and global change*, *75*:75-94.

Bailey, I.W. and Faull, A.F., 1934. The cambium and its derivative tissues: no. IX. Structural variability in the redwood, Sequoia sempervirens, and its significance in the identification of fossil woods. *Journal of the Arnold Arboretum*, *15*(3):233-254.

Barnett, J.R. and Jeronimidis, G. eds., 2003. *Wood quality and its biological basis*. CRC Press.

Bouriaud, O., Leban, J.M., Bert, D. and Deleuze, C., 2005. Intra-annual variations in climate influence growth and wood density of Norway spruce. *Tree physiology*, *25*(6): 651-660.

Bradski, G. and Kaehler, A., 2008. *Learning OpenCV: Computer vision with the OpenCV library*. O'Reilly Media, Inc..

Briggs, D., 2010. Enhancing forest value productivity through fiber quality. *Journal of Forestry*, *108*(4):174-182.

Brown, H.D. and McDowell, W.E., 1968. Status of loblolly pine die-off on the Oakmulgee District, Talladega National Forest, Alabama-1968. *US Dep. Agric. For. Serv. Rept*, (69-2):28.

Buades, A., Coll, B. and Morel, J.M., 2005, A non-local algorithm for image denoising. In *2005 IEEE Computer Society Conference on Computer Vision and Pattern Recognition (CVPR'05)*. Vol. 2. IEEE.

Burdon, R.D., Kibblewhite, R.P., Walker, J.C., Megraw, R.A., Evans, R. and Cown, D.J., 2004. Juvenile versus mature wood: a new concept, orthogonal to corewood versus outerwood, with special reference to *Pinus radiata* and *P. taeda*. *Forest Science*, *50*(4):399-415.

Cabrita, P., 2021. A model for resin flow. *Plant Cell and Tissue Differentiation and Secondary Metabolites: Fundamentals and Applications*:117-144.

Campelo, F., Nabais, C., Freitas, H. and Gutiérrez, E., 2007. Climatic significance of tree-ring width and intra-annual density fluctuations in *Pinus pinea* from a dry Mediterranean area in Portugal. *Annals of Forest Science*, *64*(2):229-238.

Cave, I.D. and Walker, J.C.F., 1994. Stiffness of wood in fast-grown plantation softwoods: the influence of microfibril angle. *Forest products journal*, *44*(5):43.

Celedon, J.M. and Bohlmann, J., 2019. Oleoresin defenses in conifers: chemical diversity, terpene synthases and limitations of oleoresin defense under climate change. *New Phytologist*, *224*(4):1444-1463.

Christiansen, E. and Ericsson, A., 1986. Starch reserves in Picea abies in relation to defence reaction against a bark beetle transmitted blue-stain fungus, Ceratocystis polonica. *Canadian Journal of Forest Research*, *16*(1):78-83.

Coley, P.D., Bryant, J.P. and Chapin, F.S., 1985. Resource availability and plant antiherbivore defense. *Science*, *230*(4728):895-899.

Coyle, D.R., Klepzig, K.D., Koch, F.H., Morris, L.A., Nowak, J.T., Oak, S.W., Otrosina, W.J., Smith, W.D. and Gandhi, K.J., 2015. A review of southern pine decline in North America. *Forest Ecology and Management*, *349*:134-148.

Coyle, D.R., Barnes, B.F., Klepzig, K.D., Koch, F.H., Morris, L.A., Nowak, J.T., Otrosina, W.J., Smith, W.D. and Gandhi, K.J., 2020. Abiotic and Biotic Factors Affecting Loblolly Pine Health in the Southeastern United States. *Forest Science*, *66*(2):145-156.

Cregg, B.M., Dougherty, P.M. and Hennessey, T.C., 1988. Growth and wood quality of young loblolly pine trees in relation to stand density and climatic factors. *Canadian Journal of Forest Research*, *18*(7):851-858.

Dahlen, J., Auty, D. and Eberhardt, T.L., 2018. Models for predicting specific gravity and ring width for loblolly pine from intensively managed plantations, and implications for wood utilization. *Forests*, *9*(6):292.

Dahlen, J., Auty, D., Eberhardt, T.L., Turnblom, E., Lowell, E., Schimleck, L. and Montes, C., 2019. Assessing the within-tree variation in stiffness from ultrasonic velocity and specific gravity measurements in Douglas-fir and loblolly pine. *Gen. Tech. Rep. FPL-GTR-272. Madison, WI: US Department of Agriculture, Forest Service, Forest Products Laboratory: 122-131*:122-131.

Dahlen, J., Nabavi, M., Auty, D., Schimleck, L. and Eberhardt, T.L., 2021. Models for predicting the within-tree and regional variation of tracheid length and width for plantation loblolly pine. *Forestry: An International Journal of Forest Research*, *94*(1):127-140.

Dalla-Salda, G., Martinez-Meier, A., Cochard, H. and Rozenberg, P., 2009. Variation of wood density and hydraulic properties of Douglas-fir (Pseudotsuga menziesii (Mirb.) Franco) clones related to a heat and drought wave in France. *Forest Ecology and Management*, *257*(1):182-189.

Downes, G.M., Hudson, I.L., Raymond, C.A., Dean, G.H., Michell, A.J., Schimleck, L.R., Evans, R. and Muneri, A., 1997. *Sampling plantation eucalypts for wood and fibre properties*. CSIRO publishing.

Eberhardt, T.L. and Samuelson, L.J., 2015. Collection of wood quality data by X-ray densitometry: a case study with three southern pines. *Wood Science and Technology*, *49*(4):739-753.

Eberhardt, T.L., Dahlen, J. and Schimleck, L., 2017. Species comparison of the physical properties of loblolly and slash pine wood and bark. *Canadian Journal of Forest Research*, *47*(11):1495-1505.

Eckhardt, L.G., Weber, A.M., Menard, R.D., Jones, J.P. and Hess, N.J., 2007. Insect-fungal complex associated with loblolly pine decline in central Alabama. *Forest Science*, *53*(1):84-92.

Eckhardt, L.G. and Menard, R.D., 2009. Declining loblolly pine stands: symptoms, causes, and management options. *AL Treasured Forest Magazine Volume XXV111, 2*:10-12.

Eckhardt, L., Sayer, M.A.S. and Imm, D., 2010. State of pine decline in the southeastern United States. *Southern Journal of Applied Forestry*, *34*(3):138-141.

Eckhardt, L.G., Menard, R.D. and Ditchkoff, S.S., 2016. Wild Pigs: inciting factor in southern pine decline? In *In: Proceedings of the 18th biennial southern silvicultural research conference. e–Gen. Tech. Rep. SRS–212. Asheville, NC: US Department of Agriculture, Forest Service, Southern Research Station.* Vol. 212.

Endara, M.J. and Coley, P.D., 2011. The resource availability hypothesis revisited: a meta-analysis. *Functional Ecology*, *25*(2):389-398.

Erbilgin, N., Cale, J.A., Hussain, A., Ishangulyyeva, G., Klutsch, J.G., Najar, A. and Zhao, S., 2017. Weathering the storm: how lodgepole pine trees survive mountain pine beetle outbreaks. *Oecologia*, *184*(2):469-478.

Erickson, H.D. and Arima, T., 1974. Douglas-fir wood quality studies part II: Effects of age and stimulated growth on fibril angle and chemical constituents. *Wood Science and Technology*, *8*(4):255-265.

Essien, C., Devkota, P., Via, B.K. and Eckhardt, L.G., 2019. Understanding relationship between the wood quality parameters and susceptibility of *Pinus taeda* to pine decline. *European Journal of Wood and Wood Products*, *77*(6):1117-1124.

Evans, R., 1994. Rapid measurement of the transverse dimensions of tracheids in radial wood sections from Pinus radiata. *Holzforschung*, *48*(2):168-172.

Evert, R.F., 2006. *Esau's plant anatomy: meristems, cells, and tissues of the plant body: their structure, function, and development*. John Wiley & Sons.

Fox, T.R., Jokela, E.J. and Allen, H.L., 2007. The development of pine plantation silviculture in the southern United States. *Journal of Forestry*, *105*(7):337-347.

Franceschi, V.R., Krokene, P., Christiansen, E. and Krekling, T., 2005. Anatomical and chemical defenses of conifer bark against bark beetles and other pests. *New Phytologist*, *167*(2):353-376.

Gaylord, M.L., Kolb, T.E., Pockman, W.T., Plaut, J.A., Yepez, E.A., Macalady, A.K., Pangle, R.E. and McDowell, N.G., 2013. Drought predisposes piñon–juniper woodlands to insect attacks and mortality. *New Phytologist*, *198*(2):567-578.

Gaylord, M.L., Kolb, T.E. and McDowell, N.G., 2015. Mechanisms of piñon pine mortality after severe drought: a retrospective study of mature trees. *Tree Physiology*, *35*(8):806-816.

Hacke, U.G., Sperry, J.S., Pockman, W.T., Davis, S.D. and McCulloh, K.A., 2001. Trends in wood density and structure are linked to prevention of xylem implosion by negative pressure. *Oecologia*, *126*(4),457-461.

Hanson, C., Yonavjak, L., Clarke, C., Minnemeyer, S., Boisrobert, L., Leach, A. and Schleeweis, K., 2010. Southern forests for the future. World Resources Institutes: Washington, DC, USA.

Harris, J.M. and Cown, D.J., 1991. Basic wood properties. *Properties and uses of New Zealand Radiata Pine [en línea]*. *Sl: Rotorua, NZ: NZ Ministry of Forestry, Forest Research Institute with assistance from the New Zealand Lottery Grants Board, c1991*.

Hasegawa, M., Takata, M., Matsumura, J., and Oda, K., 2011. Effect of wood properties on within-tree variation in ultrasonic wave velocity in softwood. *Ultrasonics*, 51(3):296-302.

Hess, N.J., Otrosina, W.J., Carter, E.A., Steinman, J.R., Jones, J.P., Eckhardt, L.G., Weber, A.M. and Walkinshaw, C.H., 2002. Assessment of loblolly pine decline in central Alabama. *Gen. Tech. Rep. SRS–48. Asheville, NC: US Department of Agriculture, Forest Service, Southern Research Station: 558-564.*

Hood, S. and Sala, A., 2015. Ponderosa pine resin defenses and growth: metrics matter. *Tree Physiology*, *35*(11):1223-1235.

Hood, S., Sala, A., Heyerdahl, E.K. and Boutin, M., 2015. Low-severity fire increases tree defense against bark beetle attacks. *Ecology*, *96*(7):1846-1855.

Jordan, L., Daniels, R.F., Clark III, A. and He, R., 2005. Multilevel nonlinear mixed-effects models for the modeling of earlywood and latewood microfibril angle. *Forest Science*, *51*(4):357-371.

Jordan, L., Clark, A., Schimleck, L.R., Hall, D.B. and Daniels, R.F., 2008. Regional variation in wood specific gravity of planted loblolly pine in the United States. *Canadian Journal of Forest Research*, *38*(4):698-710.

Kane, J.M. and Kolb, T.E., 2010. Importance of resin ducts in reducing ponderosa pine mortality from bark beetle attack. *Oecologia*, *164*(3):601-609.

Keane, R.D. and Adrian, R.J., 1992. Theory of cross-correlation analysis of PIV images. *Applied scientific research*, *49*(3):191-215.

Keeling, C.I. and Bohlmann, J., 2006. Genes, enzymes and chemicals of terpenoid diversity in the constitutive and induced defense of conifers against insects and pathogens. *New Phytologist*, *170*(4):657-675.

Kichas, N.E., Hood, S.M., Pederson, G.T., Everett, R.G. and McWethy, D.B., 2020. Whitebark pine (*Pinus albicaulis*) growth and defense in response to mountain pine beetle outbreaks. *Forest Ecology and Management*, *457*:117736.

Koch, P., 1972. *Utilization of the southern pines* (No. 420). US Southern Forest Experiment Station.

Kolosova, N. and Bohlmann, J., 2012. Conifer defense against insects and fungal pathogens. In *Growth and defense in plants* (pp. 85-109). Springer, Berlin, Heidelberg.

Kotoulas, L. and Andreadis, I., 2005, October. Image analysis using moments. In *5th Int. Conf. on Technology and Automation, Thessaloniki, Greece* Vol. 360364.

Krokene, P., Nagy, N.E. and Krekling, T., 2008. Traumatic resin ducts and polyphenolic parenchyma cells in conifers. In *Induced plant resistance to herbivory* (pp. 147-169). Springer, Dordrecht.

Krokene, P., 2015. Conifer defense and resistance to bark beetles. In *Bark beetles*:177-207. Academic press.

LaPasha, C.A. and Wheeler, E.A., 1990. Resin canals in *Pinus taeda*: longitudinal canal lengths and interconnections between longitudinal and radial canals. *IAWA journal*, *11*(3):227-238.

Larson, P.R., 1963. The indirect effect of drought on tracheid diameter in red pine. *Forest Science*, *9*(1):52-62.

Lauder, J.D., Moran, E.V. and Hart, S.C., 2019. Fight or flight? Potential tradeoffs between drought defense and reproduction in conifers. *Tree physiology*, *39*(7):1071-1085.

Levins R.,1968. Evolution in changing environments: some theoretical explorations. *Princeton* University *Press*, Princeton, NJ.

Lombardero, M.J., Ayres, M.P., Lorio Jr, P.L. and Ruel, J.J., 2000. Environmental effects on constitutive and inducible resin defenses of *Pinus taeda*. *Ecology Letters*, *3*(4):329-339.

Mason, E.G., Hayes, M. and Pink, N., 2017. Validation of ultrasonic velocity estimates of wood properties in discs of radiata pine. *New Zealand Journal of Forestry Science*, *47*(1):1-5.

McKeand, S.E., Jokela, E.J., Huber, D.A., Byram, T.D., Allen, H.L., Li, B. and Mullin, T.J., 2006. Performance of improved genotypes of loblolly pine across different soils, climates, and silvicultural inputs. *Forest Ecology and Management*, *227*(1-2):178-184.

McKinney, W., 2010~~, June~~. Data structures for statistical computing in Python. In *Proceedings of the 9th Python in Science Conference*.Vol. 445.

McNulty, S.G., Vose, J.M. and Swank, W.T., 1996. Loblolly pine hydrology and productivity across the southern United States. *Forest Ecology and Management*, *86*(1-3):241-251.

Megraw, R.A., 1985. *Wood quality factors in loblolly pine: the influence of tree age, position in tree, and cultural practice on wood specific gravity, fiber length, and fibril angle*. TAPPI Press.

Megraw, R.A., Bremer, D., Leaf, G. and Roers, J., 1999. Stiffness in loblolly pine as a function of ring position and height, and its relationship to microfibril angle and specific gravity. In *Workshop IUFRO S* (Vol. 5, pp. 01-04).

Melo, R.R., 2015. Radial and longitudinal variation of *Pinus taeda* L. wood basic density in different ages. *Revista de Ciências Agrárias Amazonian Journal of Agricultural and Environmental Sciences*, *58*(2):192-197.

Meylan, B.A., 1972. The influence of microfibril angle on the longitudinal shrinkage-moisture content relationship. *Wood Science and Technology*, *6*(4):293-301.

Miller, R.H. and Berryman, A.A., 1986. Carbohydrate allocation and mountain pine beetle attack in girdled lodgepole pines. Canadian Journal of Forest Research, 16(5):1036-1040.

Moran, E., Lauder, J., Musser, C., Stathos, A. and Shu, M., 2017. The genetics of drought tolerance in conifers. *New Phytologist*, *216*(4):1034-1048.

Moreira, X., Zas, R. and Sampedro, L., 2012. Methyl jasmonate as chemical elicitor of induced responses and anti-herbivory resistance in young conifer trees. In *Plant defence: Biological control* (pp. 345-362). Springer, Dordrecht.

Motwani, M.C., Gadiya, M.C., Motwani, R.C. and Harris, F.C., 2004, September. Survey of image denoising techniques. In *Proceedings of GSPX* (Vol. 27, pp. 27-30). Proceedings of GSPX.

Munsell, J.F. and Fox, T.R., 2010. An analysis of the feasibility for increasing woody biomass production from pine plantations in the southern United States. *Biomass and Bioenergy*, *34*(12):1631-1642.

Nagy, N.E., Franceschi, V.R., Solheim, H., Krekling, T. and Christiansen, E., 2000. Wound-induced traumatic resin duct development in stems of Norway spruce (Pinaceae): anatomy and cytochemical traits. *American Journal of Botany*, *87*(3):302-313.

Novaes, E., Kirst, M., Chiang, V., Winter-Sederoff, H. and Sederoff, R., 2010. Lignin and biomass: a negative correlation for wood formation and lignin content in trees. *Plant Physiology*, *154*(2):555-561.

Oliphant, T.E., 2006. *A guide to NumPy* (Vol. 1, p. 85). USA: Trelgol Publishing.

Oswalt, S.N., Smith, W.B., Miles, P.D. and Pugh, S.A., 2019. Forest resources of the United States, 2017: A technical document supporting the Forest Service 2020 RPA Assessment. *Gen. Tech. Rep. WO-97. Washington, DC: US Department of Agriculture, Forest Service, Washington Office.*, *97*.

Otrosina, W.J., Bannwart, D. and Roncadori, R.W., 1999. Root-infecting fungi associated with a decline of longleaf pine in the southeastern United States. *Plant and Soil*, *217*(1):145-150.

Perez, D.D.S. and Fauchon, T., 2003. Wood quality for pulp and paper. *Wood quality and its biological basis*, pp.157-186.

Phillips, K.M., 2002. *Modeling within-tree changes in wood specific gravity and moisture content for loblolly pine in Georgia* (Thesis, University of Georgia).

Pinheiro J, Bates D, DebRoy S, Sarkar D, R Core Team. 2021. *nlme: Linear and Nonlinear Mixed Effects Models*. R package version 3.1-152, https://CRAN.R-project.org/package=nlme

Pittermann, J., Sperry, J.S., Hacke, U.G., Wheeler, J.K. and Sikkema, E.H., 2006a. Inter-tracheid pitting and the hydraulic efficiency of conifer wood: the role of tracheid allometry and cavitation protection. *American Journal of Botany*, *93*(9):1265-1273.

Pittermann, J., Sperry, J.S., Wheeler, J.K., Hacke, U.G. and Sikkema, E.H., 2006b. Mechanical reinforcement of tracheids compromises the hydraulic efficiency of conifer xylem. *Plant, Cell & Environment*, *29*(8):1618-1628.

Pizer, S.M., 1990. Contrast-limited adaptive histogram equalization: Speed and effectiveness. In *Proceedings of the First Conference on Visualization in Biomedical Computing*. Vol. 337.

Raffa, K.F., 2014. Terpenes tell different tales at different scales: glimpses into the chemical ecology of conifer-bark beetle-microbial interactions. *Journal of Chemical Ecology*, *40*(1):1-20.

Rais, N. B., Hanif, M. S., & Taj, I. A. 2004. Adaptive thresholding technique for document image analysis. In *8th International Multitopic Conference, 2004. Proceedings of INMIC 2004*. IEEE.

Raybaut, P., 2009. Spyder-documentation. *Available online at: pythonhosted. org*.

Richter, H. G., Grosser, D., Heinz, I., & Gasson, P. E. (Eds.)., 2004. IAWA list of microscopic features for softwood identification. *IAWA Journal*, *25*(1):1-70.

Rossi, S., Simard, S., Rathgeber, C.B., Deslauriers, A. and De Zan, C., 2009. Effects of a 20-day-long dry period on cambial and apical meristem growth in Abies balsamea seedlings. *Trees*, *23*(1):85-93.

R Core Team., 2021. R: A language and environment for statistical computing. R Foundation for statistical computing, Vienna, Austria. URL https://www.R-project.org/.

RStudio Team., 2020. RStudio: Integrated Development for R. RStudio, Inc., Boston, MA URL http://www.rstudio.com/.

Ruel, J.J., Ayres, M.P. and Lorio, Jr, P.L., 1998. Loblolly pine responds to mechanical wounding with increased resin flow. *Canadian Journal of Forest Research*, *28*(4):596-602.

Sasi, N.M. and Jayasree, V.K., 2013. Contrast limited adaptive histogram equalization for qualitative enhancement of myocardial perfusion images. *Engineering*, *5*(10):326-331.

Schimleck, L., Antony, F., Dahlen, J. and Moore, J., 2018. Wood and fiber quality of plantation-grown conifers: A summary of research with an emphasis on loblolly and radiata pine. *Forests*, *9*(6):298.

Schimleck, L.R., Antony, F., Mora, C. and Dahlen, J., 2020. Whole-tree tracheid property maps for loblolly pine at different ages. *Wood Science and Technology*, *54*(3):683-701.

Schimleck, L.R., Antony, F., Mora, C. and Dahlen, J., 2021. Mapping and modeling within-tree variation for loblolly pine pulp yield and lignin content. *SN Applied Sciences*, *3*(4):1-14.

Schmid, J.N., 2017. Using Google Earth Engine for Landsat NDVI time series analysis to indicate the present status of forest stands. *Georg-August-Universität Göttingen: Basel, Switzerland*.

Schomaker, M.E., Zarnoch, S.J., Bechtold, W.A., Latelle, D.J., Burkman, W.G. and Cox, S.M., 2007. Crown-condition classification: a guide to data collection and analysis. *Gen. Tech. Rep. SRS-102. Asheville, NC: US Department of Agriculture, Forest Service, Southern Research Station. 78:* 102.

Senft, J.F. and Bendtsen, B.A., 1986. Juvenile wood: processing and structural products considerations. In *Series: Conference Proceedings*.

Serra, J. (1982) Image Analysis and Mathematical Morphology. Academic Press, New York.

Sjöstrom, E., 1993. *Wood chemistry: fundamentals and applications*. Gulf professional publishing.

Smook, G.A., 2002. Characteristics of wood and wood pulp fibers. *SMOOK, GA Handbook for pulp & paper technologists. 3rd. ed. Vancouver: Angus Wilde Publications*, pp.10-19.

Taras, M.A., 1956. Buying pulpwood by weight as compared with volume measure. *USDA Forest Service, Southeastern Forest Experiment Station, Old Station Paper, OSP-074, 13 p., 74.*

Teague, M.R., 1980. Image analysis via the general theory of moments. *Josa*, *70*(8):920-930.

Todoroki, C.L., Low, C.B., McKenzie, H.M. and Gea, L.D., 2015. Radial variation in selected wood properties of three cypress taxa. *New Zealand Journal of Forestry Science*, *45*(1): 1-14.

Van Rossum, G. 2007. Python Programming Language. In USENIX annual technical conference.Vol. 41.

Wear, D.N. and Greis, J.G., 2012. The southern forest futures project: summary report. *Gen. Tech. Rep. SRS-GTR-168. Asheville, NC: USDA-Forest Service, Southern Research Station. 54 p., 168*:1-54.

Wickham, H., Chang, W. and Wickham, M.H., 2016. Package 'ggplot2'. *Create Elegant Data Visualisations Using the Grammar of Graphics. Version*, *2*(1):1-189.

Wickham, H., François, R., Henry, L. and Müller, K., 2018. Dplyr: A grammar of data manipulation (R package version 0.7. 6)[Computer software].

Wiedenhoeft, A.C. and Miller, R.B., 2002. Brief comments on the nomenclature of softwood axial resin canals and their associated cells. *IAWA journal*, *23*(3):299-303.

Wimmer, R. and Grabner, M., 1997. Effects of climate on vertical resin duct density and radial growth of Norway spruce [Picea abies (L.) Karst.]. *Trees*, *11*(5):271-276.

Wimmer, R., Grabner, M., Strumia, G. and Sheppard, P.R., 1999. Significance of vertical resin ducts in the tree rings of spruce. *Tree-ring analysis: biological, methodological and environmental aspects. Edited by R. Wimmer and RE Vetters. CABI Publishing, Oxon, UK*:107-118.

Wodzicki, T.J. and Zajączkowski, S., 1983. Variation of seasonal cambial activity and xylem differentiation in a selected population of Pinus silvestris L. *Folia Forestalia Polonica Series A*, *25*:5-23.

Wodzicki, T.J., 2001. Natural factors affecting wood structure. *Wood Science and Technology*, *35*(1-2):5-26.

Wu, H. and Hu, Z.H., 1997. Comparative anatomy of resin ducts of thePinaceae *Trees*, *11*(3): 135-143.

Xu, J., Lu, J., Evans, R. and Downes, G.M., 2014. Relationship between ring width and tracheid characteristics in Picea crassifolia: implication in dendroclimatology. *Bioresources*, 9(2):2203-2213.

Yoo, J.C. and Han, T.H., 2009. Fast normalized cross-correlation. *Circuits, systems and signal processing*, *28*(6):819-843.

Zhao, D., Kane, M., Teskey, R., Fox, T.R., Albaugh, T.J., Allen, H.L. and Rubilar, R., 2016. Maximum response of loblolly pine plantations to silvicultural management in the southern United States. *Forest Ecology and Management*, *375*:105-111.

Zhao, D., Bullock, B.P., Montes, C.R., Wang, M., Greene, D. and Sutter, L., 2019. Loblolly pine outperforms slash pine in the southeastern United States–A long-term experimental comparison study. *Forest ecology and management*, *450*:117532.

Zhao, S. and Erbilgin, N., 2019. Larger resin ducts are linked to the survival of lodgepole pine trees during mountain pine beetle outbreak. *Frontiers in Plant Science*, *10*:1459.

Zink-Sharp, A., 2003. The mechanical properties of wood. *Wood Quality and its Biological Basis. Blackwell Publishing-CRC Press. Biological Sciences Series. Boca Raton, Fla., EUA*:187-210.

Zobel, B.J. and Sprague, J.R., 2012. *Juvenile wood in forest trees*. Springer Science & Business Media.

Zobel, B.J. and van Buijtenen, J.P., 2012. *Wood variation: its causes and control*. Springer Science & Business Media.

Zulak, K.G. and Bohlmann, J., 2010. Terpenoid biosynthesis and specialized vascular cells of conifer defense. *Journal of Integrative Plant Biology*, *52*(1):86-97.